UTRECHT UNIVERSITY

INSTITUTE OF THEORETICAL PHYSICS

MASTER THESIS

A holographic investigation of magnetically induced quantum critical points in 2+1-dimensions

Author:
Claire Moran

Supervisor:
Dr. Umut Gürsoy

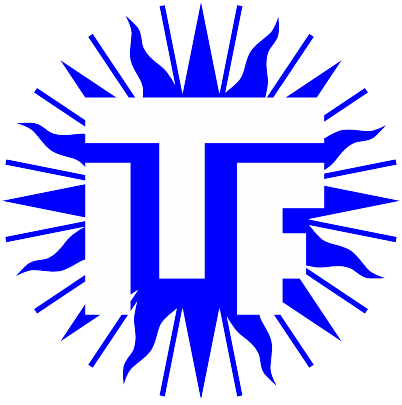

July 14, 2019

"Somewhere, something incredible is waiting to be known."

Carl Sagan

UTRECHT UNIVERSITY

Abstract

Master of Theoretical Physics

A holographic investigation of magnetically induced quantum critical points in 2+1-dimensions

by Claire Moran

We study a 2+1-dimensional quantum critical system under the influence of an external magnetic field and at finite chemical potential using holography. The gauge theory is related to the ABJM model deformed by a bosonic gauge invariant triple trace operator, and is non-conformal. The gravity dual is based on a 4-dimensional $\mathcal{N} = 2$ Fayet-Iliopoulos gauged supergravity, and black brane and thermal gas solutions are considered. The system undergoes a phase transition at some B_c, resulting in a line of quantum critical points. We investigate these points and the surrounding region using the quasinormal modes of the black brane solution. We find evidence of the quantum phase transition within the behaviour of the fundamental mode, and we extract the $T - B$ phase diagram in one case of the parameter conditions.

Acknowledgements

Thanks to my classmates for many fun hours spent in the Master room providing some comic relief from the madness of this year. A big thank you to Domingo Gallegos Pazos who spent more time than he should have helping me figure out Mathematica packages. Also thank you to Govert Nijs, who helped me with some things even when he wasn't on the continent.

Contents

Chapter 1

Introduction: Strongly coupled systems

Strongly interacting many body systems are a very important but poorly understood area in physics. The usual techniques which have gotten us so far in physics, such as perturbation theory and weak coupling approximations, cannot be used in these systems. Strongly interacting systems are prevalent throughout nature, which can be modelled by these systems from the high energy regime (low energy quantum chromodynamics), to the low energy regime (high temperature superconductors, quantum critical systems, etc.). Therefore, given the abundance and fundamental nature of these systems, it is paramount that we develop methods to explore and understand them.

The strongly coupled system this thesis will be concerned with, is a quantum critical system. Quantum criticality is currently an important topic in physics, as it is thought that it is crucial in the understanding of several open problems, such as high T_c superconductivity. In particular, we will study a magnetically induced quantum critical point (QCP) using holography. Holography, or the gauge/gravity duality was first realised through Maldacena's AdS/CFT conjecture. In one limit, it reveals a correspondence between strongly coupled gauge theories and weakly coupled gravity theories, and thus provides us with a powerful means to study these strongly coupled theories.

1.1 Why condensed matter?

In condensed matter physics, there are many strongly coupled systems that cannot be properly understood through the traditional approaches to problems in condensed matter physics (using weak approximations etc.). The AdS/CFT correspondence presents a unique way to tackle these problems and obtain results that would otherwise be very difficult to determine. Furthermore, since these strongly coupled systems can be constructed and experimented on in a laboratory, they may provide us with the means to experimentally realise concepts from high energy physics.

Many condensed matter systems provide a so-called top-down approach to the AdS/CFT correspondence; where we know the precise form of the duality, namely we can write down a Lagrangian on the field theory side and the gravity dual is well understood in the supergravity limit. This is opposed to bottom-up approach in which the exact duality is not known, instead the duality used is based on things such as symmetry arguments, so it is similar in the necessary ways to the actual systems in question. With the top-down approach, precise questions can be asked and answered, so this application of the AdS/CFT correspondence is very promising and powerful.

Finally, results we obtain from the correspondence about the strongly coupled system do not only have implications for said system, they can also have consequences for the gravity dual. For instance, seeking a dual description of superconductivity one realises that there might be loopholes in black hole 'no-hair' theorems and one is led to new types of black hole solutions [1]. Evidently, this dual perspective can lead to finding new results and possibilities on both sides, a "buy one get one free" deal offered by nature to those clever enough!

1.1.1 Quantum criticality

An example of strongly coupled condensed matter systems that can be studied using holographic techniques are quantum critical systems, the type of condensed matter system that will be investigated in this thesis. Quantum phase transitions are continuous phase transitions occurring at zero temperature, through variation of another non-termal parameter of the theory, such as the chemical potential or magnetic field. The phase transition in these cases are driven by quantum fluctuations due to the Heisenberg uncertainty principle, since at $T = 0$ there can be no thermal fluctuations.

The quantum phase transition occurs at some critical value in the varying parameter, known as the quantum critical point (QCP). There are two types of QCPs, shown below in figure . The first on the left is known as a level crossing, this occurs when the parameter controlling the phase transition couples to a conserved quantitiy. In this case an excited energy level becomes the ground state at the QCP, leading to a non-analyticiy in the ground state energy. The second type shown on the right, is known as an avoided level crossing, which occurs in the infinite lattice limit. As the lattice size increases the curves become sharper, with $\Delta E \to 0$, and the non-analyticity occurs at the QCP. This type of QCP is much more common than the first, and as we will see this is the kind exhibited in our system.

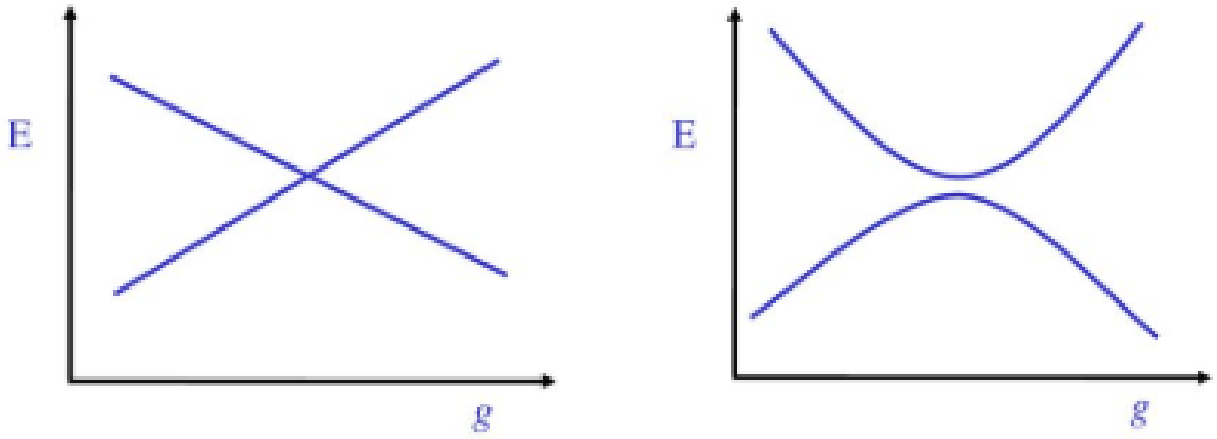

FIGURE 1.1: The two types of QCPs. On the left we have a level crossing, and on the right an avoided level crossing. The latter is more common and is the type that occurs in our system.

A particular class of quantum phase transitions are those which are of second order, where the non-analyticity manifests itself in the second derivative of the free energy. In general for a second order quantum phase transition, as the QCP is approached the characteristic energy scale of the system vanishes and the characteristic lengthscale diverges, and so the system becomes scale invariant. At this point the system is also invariant under rotations, translations, time translations and dilatations. So at the QCP the effective field theory is scale invariant, i.e. a *conformal field theory*, we will discuss conformal field theories in sufficient detail in chapter two. We will also see later, that a metric that obeys all of these symmetries is precisely the Anti-de Sitter(AdS) spacetime metric, and so it is already apparent why the correspondence will be useful to study such systems.

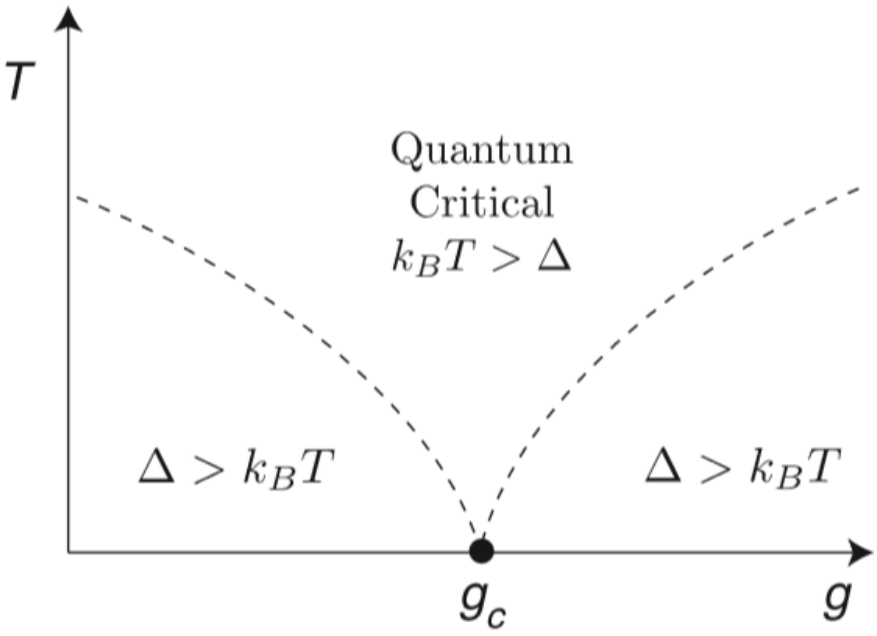

FIGURE 1.2: A typical phase diagram near a quantum critical point. T is the temperature, g is another parameter of the system such as pressure or magnetic field, and Δ is the characteristic energy scale. A clear division of the phase diagram into different regimes can be observed. g_c defines the QCP, separating quantum ordered and quantum disordered states. As this point is approached the energy scale vanishes. The quantum critical region in which the quantum fluctuations dominate can be seen. This image is taken from [2]

The typical phase diagram for a quantum phase transition is divided into two main regions defined by the relationship between the characteristic energy scale of the system and thermal energy, as shown in figure 1.2. The first regime is defined when $k_BT < \Delta$, where the characteristic energy is dominating the thermal energy. In this region, the thermal energy is not enough to excite the quantum states into a superposition of states, where quantum effects are important. As a result, the system is effectively classical in this region, and we can deal with the dynamics as so. Another property of this region is that the equilibration timescale, the time it takes for the perturbed system to return to equilibrium, is given by $\tau_{eq} \gg \frac{\hbar}{k_BT}$.

The second regime is known as the quantum critical region, in which $k_BT > \Delta$. Here, the thermal energy is dominating the characteristic energy. Consequently, thermal fluctuations have enough energy to excite the quantum states into a superposition and so quantum effects become non-negligible, and the effective field theory is no longer semi-classical. We need an effective field theory that takes these quantum effects into account. For strongly interacting quantum critical systems, the timescale is given by $\tau_{eq} \sim \frac{\hbar}{k_BT}$, so quite different to the other region. This will be useful for us later, but it should be stressed that the exact proportionality in not known. The equation for τ is given by,

$$\tau_{eq} = C_{eq}\frac{\hbar}{k_BT}, \tag{1.1}$$

where C_{eq} is a number that doesn't depend on the microscopic details of the system. We do not know what C_{eq} is for our system, and this lead to some limitations that we will see later.

QCP's are highly interesting in that they can dominate regions of the phase diagram beyond the point at which the energy fluctuations vanish, namely they influence the quantum critical region. As a result, we can consider the dynamics inside the quantum critical as also being governed by a conformal field theory. The quantum fluctuations at the QCP that drive the phase transition are presently not

well understood, and in order to develop a satisfactory theory of quantum phase transitions, these fluctuations must be comprehended.

Outside of AdS/CFT, there are presently no models of strongly coupled quantum criticality in 2+1 dimensions in which analytic results can be obtained. Therefore this is a very promising and important application of the AdS/CFT correspondence, which we will explore in this thesis.

For more information on quantum critical systems and quantum phase transitions, a comprehensive overview of the subject can be found at [2].

1.1.2 Why *this* condensed matter system

Now we will introduce the condensed matter system that we are considering, and explain why this one is interesting to study holographically.

The system we consider is a (2+1)-dimensional gauge theory, at finite potential and magentic field. In particular, it is a strongly-coupled, non-conformal theory, related to the ABJM model deformed by a bosonic gauge invariant triple trace operator. This operator introduces the instability in the system initiating the RG flow, and hence breaking the conformality. This system undergoes a phase transition at some critical value of the magnetic field, and we are interested in studying these critical points and the surrounding regions.

This model is interesting to study, as it is one in which the top-down approach can be utilized. In particular, it is one of the few involving an external magnetic field for which the precise duality is known, and where the dual gravity solutions are analytic. As a result of this, we can can ask more detailed questions and obtain the answers, for example one could compute the thermal and electrical conductivities of the system, among other things.

As mentioned earlier, (2+1)-dimensional quantum critical systems do not have any effective models outside of AdS/CFT, and it is believed that high T_c superconductors may have their properties rooted in the presence of a quantum critical point. The multi trace type operator introduced in this system, is also important in the study of holographic superconductors, so studying these kinds of systems is promising for the development of a description of high T_C superconductors.

1.2 Layout of the thesis

Hopefully this chapter has provided enough motivation for why we want to study condensed matter using holography, and in particular the condensed matter system we are investigating. So the next step is to overview the necessary background information that was needed for this thesis. In chapter two, the ingredients of the AdS/CFT correspondence will be introduced and explained, and then the correspondence itself will be detailed. Chapter three will briefly discuss some important features of the correspondence that are necessary for our purposes, and then chapter four will outline the problem, the systems we are considering, what we did, and the results we obtained. Finally then in chapter five we will summarize these results again, detail the conclusions, and discuss what should be done next.

Chapter 2

The AdS/CFT correspondence

The purpose of this chapter will be to present the correspondence as proposed by Maldacena [3], where an exact equivalence is made between type IIB superstring theory compactified on $AdS_5 \times S^5$, and $\mathcal{N} = 4$ Super Yang-Mills theory in $3+1$ dimensions. The corresponence is a realisation of the holographic principle, first proposed by t'Hooft, which states that there is an equivalence between a non-Abelien gauge theory at large N and a string theory, which will be discussed below. In order to get to the correspondence we must first review the basic ingredients of the duality: Anti-de Sitter spacetime and conformal field theories. We will begin by introducing these two topics in their relevant capacity, and then move onto the topics that will eventually lead us to the correspondence between them, namely superstring theory and supergravity. From there we will be able to detail the correspondence and discuss its consequences.

2.1 Large N expansion and holography

First proposed by 't Hooft in [4], is the idea that gauge theories at large N, where N is the rank of the gauge group, is equivalent to a string theory. The AdS/CFT correspondence is this first direct realisation of this duality, giving the precise mapping.

The perturbative expansion of a large N guage theory in $\frac{1}{N}$ and g^2_{YM} has the form

$$Z = \sum_{g \geq 0} N^{2-2g} f_g(\lambda), \tag{2.1}$$

where f_g is a polynomial in the 't Hooft coupling $\lambda = g^2_{\text{YM}}$, and the $N \to \infty$ limit has been taken while keeping λ fixed. Looking closely at this we see that the power of N is precisely the Euler characteristic, where g is the genus of the surface, and so we see that this looks exactly like the string theory perturbative expansion,

$$Z = \sum_{g \geq 0} g_s^{2g-2} Z_g, \tag{2.2}$$

where $g_s = \frac{1}{N}$ is the string coupling.

The holographic principle has its origins in the study of black hole thermodynamics, where [5] and [6] showed that black holes can be have as thermodynamic systems. It was found that the entropy of the black hole is directly proportional to the area of horizon, and this only really makes sense if we can form an equivalence between a gravity theory in d dimensions and a local field theory in $d-1$ dimensions. Consider that an area in d dimensions is the same as the volume in $d-1$ dimensions, and we know from statistical mechanics that a field theory in $d-1$ dimensions will have an entropy proportional to its area. From this, we can conjecture that since a black hole in d dimensions has entropy proportional to its area, it must be equivalent to a $d-1$ dimensional field theory.

This is where the term "holographic principle" comes from; a hologram is a 2-dimensional object that contains all the information to form a 3-dimensional object, and like this all the information of a d-dimensional black hole is contained within a $d-1$-dimensional field theory.

As we will see, the AdS/CFT correspondence fulfils the definition of the holographic principle, as it conjectures that 5-dimensional quantum gravity is equivalent to a 4-dimensional local field theory.

2.2 Anti-de Sitter spacetime

Anti-de Sitter, which from here on will be referred to as AdS spacetime, is a maximally symmetric spacetime with negative cosmological constant. In $(d+1)$-dimensions, the AdS_{d+1} hypersurface is given by

$$\bar{\eta}_{NM}X^N X^M = -(X^0)^2 + \sum_{i=1}^{d}(X^i)^2 - (X^{d+1})^2 = -L^2, \tag{2.3}$$

where $\bar{\eta}$ =diag$(-1,+1,...,+1,-1)$ and $M,N \in \{0,...,d+1\}$ This can be embedded into $(d+2)$-dimensional Minkowski spacetime with metric,

$$ds^2 = -(dX^0)^2 + (dX^1)^2 + ... + (dX^d)^2 - (dX^{d+1})^2 = \bar{\eta}_{NM}dX^M dX^N \tag{2.4}$$

A useful and convenient coordinate system for us to use will be the Poincaré patch coordinates, where we parameterise as follows,

$$X^0 = \frac{L^2}{2r}(1 + \frac{r^2}{L^4}(\bar{x}^2 - t^+L^2)), \tag{2.5}$$

$$X^i = \frac{rx^i}{L}, i \in \{1,...,d-1\}, \tag{2.6}$$

$$X^d = \frac{L^2}{2r}(1 + \frac{r^2}{L^4}(\bar{x}^2 - t^+L^2)), \tag{2.7}$$

$$X^{d+1} = \frac{rt}{L}. \tag{2.8}$$

Due to the choice of coordinates $r > 0$, only one half of the AdS_{d+1} is covered. The metric in Poincaré coordinates is

$$ds^2 = \frac{L^2}{r^2}dr^2 + \frac{r^2}{L^2}(\eta_{\mu\nu}dx^\mu dx^\nu), \tag{2.9}$$

where $\mu = 0,...,d$, $x^0 = t$, and $\eta_{\mu\nu} = \text{diag}(-1,+1,+1,...,+1)$. In these coordinates AdS-spacetime can be seen as flat spacetime with $(\bar{x},t)$ coordinates, combined with an extra warped direction r. As the boundary is approached, i.e. $r \to \infty$, there is a second order pole in the metric in the g_{ii} components of the metric. This is a general feature: any asymptotically AdS spacetime metrics will always have quadratic divergences in a certain direction, for a particular value of the radial direction, say $r = r^*$, and this r^* is the conformal boundary of the spacetime. The conformal boundary is important as this is where the dual field theory lives.

A slightly more convenient way for us to express the Poincaré coordinates is by inverting the r-coordinate, such that $z = -\frac{L^2}{r}$. Now the metric reads,

$$ds^2 = \frac{L^2}{z^2}(dz^2 + \eta_{\mu\nu}dx^\mu dx^\nu), \tag{2.10}$$

and the horizon is located at $z \to \infty$, and the conformal boundary at $z = 0$.

2.3 Conformal field theory

In quantum field theories, symmetries play an important role, in particular we have seen how Lorentz and Poincaré symmetries affect our understanding of the theory. Another symmetry which one could try to add to the boots, rotations, and translations of the Poincaré group is that of scale invariance. The group containing both scale invariance as well as Poincaré invariance is known as the full conformal group. The conformal group is the group of transformations that preserve angles, or it can also be sen as those coordinate transformations which leave the metric invariant up to a scale factor, and these transformations are known as conformal transformations. A field theory that is invariant under these conformal transformations is known as a conformal field theory(CFT). As we will see, $d = 4, \mathcal{N} = 4$ supersymmetric Yang-Mills theory is such a field theory.

2.3.1 The conformal algebra and group

As stated above a conformal transformation is a coordinate transformation, $\sigma^\alpha \mapsto \tilde{\sigma}^\alpha(\sigma)$, which leaves the metric invariant up to a scale factor,

$$g_{\alpha\beta} \mapsto \Omega(\sigma)^2 g_{\alpha\beta}(\sigma), \tag{2.11}$$

where $\alpha, \beta = \{0, 1, ..., d-1\}$. We will now investigate what these transformations are in the case of flat spacetime, $g_{\alpha\beta} = \eta_{\alpha\beta}$. Taking an infinitesimal transformation $x \mapsto \tilde{x} = x^\alpha + \epsilon^\alpha(x)$, the metric then transorms as

$$\eta_{\alpha\beta} \mapsto \eta_{\alpha\beta} + \partial_\alpha \epsilon_\beta + \partial_\beta \epsilon_\alpha. \tag{2.12}$$

Now, equation 2.12 implies that the conformal transformation has to satisfy

$$\partial_\alpha \epsilon_\beta + \partial_\beta \epsilon_\alpha = f(x)\eta_{\alpha\beta}, \tag{2.13}$$

where f(x) is some function. We can then solve for $f(x)$ by contracting both sides with the metric, then we eventually find, that for d dimensions, an infinitesimal transformation is conformal if $\epsilon(x)$ satisfies

$$(\eta_{\alpha\beta}\partial_\gamma\partial^\gamma + (d-2)\partial_\alpha\partial_\beta)\partial \cdot \epsilon = 0. \tag{2.14}$$

We will be concerned with spacetimes with $d > 2$, in which case the conformal equation 2.14 is solved if ϵ is of at most second order. From this one can determine the generators of the group, which are found to be

- $P_\alpha \rightarrow$ translations
- $J_{\alpha\beta} \rightarrow$ Lorentz transformations (boosts and rotations)
- $D \rightarrow$ dilatation
- $K_\alpha \rightarrow$ special conformal transformations

These generators obey the commutation relations of the Poincaré algebra as well as new ones

$$\begin{aligned} [J_{\alpha\beta}, J_{\gamma\sigma}] &= i(\eta_{\alpha\gamma}J_{\beta\sigma} + (\alpha \Leftrightarrow \beta, \gamma \Leftrightarrow \sigma) - (\alpha \Leftrightarrow \beta) - (\gamma \Leftrightarrow \sigma)), \\ [J_{\alpha\beta}, K_\gamma] &= i(\eta_{\alpha\gamma}K_\beta - \eta_{\beta\gamma}K_\alpha), \\ [D, P_\alpha] = iP_\alpha, \quad [D, K_\alpha] &= -iK_\alpha, \quad [D, J_{\alpha\beta}] = 0, \\ [K_\alpha, K_\gamma] = 0, \quad [K_\alpha, P_\beta] &= 2i(\eta_{\alpha\beta}D - J_{\alpha\beta}). \end{aligned} \tag{2.15}$$

These generators give us the usual finite transformations from the Poincaré group; translations (P_α), Lorentz transformations ($J_{\alpha\beta}$), as well as new ones; dilatations/scalings (D)

$$x^\alpha \mapsto \lambda x^\alpha, \tag{2.16}$$

and special conformal transformations (K_α),

$$x^\alpha \mapsto \frac{x^\alpha + b^\alpha x^2}{1 + 2b \cdot x + b^2 x^2}. \tag{2.17}$$

The confromal algebra is isomorphic to the algebra $\mathbf{so}(d,2)$, provided we make the following identifications, where the barred terms are the generators of $\mathbf{so}(d,2)$:

$$\begin{aligned} \bar{J}_{d(d+1)} &= -D, \\ \bar{J}_{\alpha d} &= \frac{1}{2}(K_\alpha - P_\alpha), \\ \bar{J}_{\alpha(d+1)} &= \frac{1}{2}(P_\alpha + K_\alpha), \end{aligned} \tag{2.18}$$

where $\alpha \in \{0, ..., d-1\}$. The fact that the conformal algebra is isomorphic to the algebra $\mathbf{so}(d,2)$ is important as this is the isometry group of AdS space.

2.3.2 Field content, correlators, and OPEs

The next thing to look at are the representations of the conformal group, so we can determine the field content of our theory.

Under a scaling transformation, a field $\phi(x)$ will transform as,

$$\phi(\lambda x) = \lambda^{-\Delta}\phi(x), \tag{2.19}$$

where Δ is the scaling dimension.

Commutation relations 2.13 imply that P_μ and K_μ increase and decrease the scaling dimension respectively. It can be shown that for a CFT to be unitary, there must be a lower bound on the scaling dimension of its fields, therefore it follows that there exist fields of the lowest possible scaling dimension in each representation. These fields will be annihilated at $x = 0$ by K_μ, these fields are called the conformal *primary fields*, and they satisfy the commutation relation,

$$[K_\mu, \Phi(0)] = 0. \tag{2.20}$$

All other fields can then be obtained from the primary fields, by acting on them with P_μ, and the commutation relations for these primary fields are as follows,

$$\begin{aligned} [P_\mu, \Phi(x)] &= -i\partial_\mu \Phi(x) \\ [D, \Phi(x)] &= -i\Delta\Phi(x) \\ [J_{\mu\nu}, \Phi(x)] &= -\mathcal{J}_{\mu\nu}\Phi(x) + i(x_\mu\partial_\nu - x_\nu\partial_\mu) \\ [K_\mu, \Phi(x)] &= (i(-x^2\partial^\mu + 2x_\mu x^\rho\partial_\rho + 2x_\mu\Delta) - 2x^\nu\mathcal{J}_{\mu\nu})\Phi(x), \end{aligned} \tag{2.21}$$

where $\mathcal{J}_{\mu\nu}$ are the finite-dimensional representation of the Lorentz group.

Now we can look to the observables of the theory; the correlation functions. The conformal invariance of the theory will invoke restrictions on these observables, where the classical invariance of the action under conformal transformations leads to Ward identities on the quantum level i.e. in the correlation functions.

Using the invariance under dilatations and specialconformal transformations, it can be shown that the two-point function of two scalar primary operators is,

$$\langle \Phi(x_1)\Phi(x_2)\rangle = \frac{A_{12}}{|x_1 - x_2|^{\Delta}}, \tag{2.22}$$

where A_{12} is just a normalisation constant. Similarily, the three-point function can be found to be,

$$\langle \Phi(x_1)\Phi(x_2)\Phi(x_3)\Phi(x_4)\rangle = \frac{\lambda_{123}}{x_{12}^{\Delta-2\Delta_3} x_{23}^{\Delta-2\Delta_1} x_{13}^{\Delta-2\Delta_2}}, \tag{2.23}$$

where $\Delta = \sum_i \Delta_i$ and $x_{ij} =\mid x_i - x_j \mid$, and λ_{123} is again a normalisation constant. Now that we have the correlation functions we can introduce a useful concept in CFTs: operator product expansions (OPEs), which are defined by,

$$O_i(x_1)O_j(x_2) = \sum_k C_{ij}^k (x_1 - x_2) O^k(x_2). \tag{2.24}$$

OPEs turn out to contain the same information as the correlation functions, as well as showing us how the operators transform under the symmetries.

Finally, another very useful tool from CFTs is the state-operator correspondence, which provides us with an invertible map between states $|O\rangle$, and local operators O,

$$|O\rangle = \lim_{x\to 0} O(x)|0\rangle. \tag{2.25}$$

2.3.3 Superconformal field theory

We can further generalise the Poincaré algebra by introducing supersymmetry algebra, which adds fermionic operators Q_α^a to the story, and therefore introducing anti-commutation relations. The superconformal algebra will contain the usual generators of the conformal group, $J_{\mu\nu}$,P_μ,D, and K_μ, as well as the supersymmetry supercharges Q_α^a and $\bar{Q}_{\dot\alpha}^a$, where $a = 1, ..., \mathcal{N}$ is the number of independent supersymmetries and α,$\dot\alpha$ are the $SL(2,\mathbb{C})$ indices, taking values 1,2.

However, it is necessary to indroduce further generators to the superconformal group; further fermionic supercharges denoted by S_α^a and $\bar{S}_{\dot\alpha}^a$. These superconformal algebras exist only in $d \leq 6$, and their commutation relations, including (2.13) are,

$$\begin{gathered}[D,Q] = -\frac{i}{2}Q, \quad [D,S] = \frac{i}{2}S, \quad [K,Q] \simeq S, \quad [P,S] \simeq Q, \\ \{Q,Q\} \simeq P, \quad \{S,S\} \simeq K, \quad [Q,S] \simeq J + D + R,\end{gathered} \tag{2.26}$$

where R is the R-symmetry, curly brackets indicate anti-commutation relations, and all indices have been suppressed.

As in the previous section, when finding the representations of the algebra, in this case the superconformal algebra, we find there are operators which have the lowest dimension Δ, reffered to as *superconformal primary operators*. The unitarity implies that these operators must satisfy,

$$[S_{\dot\alpha}^a, O\} = 0, \quad [\bar{S}_{a\dot{\alpha}}, O], \tag{2.27}$$

where the final brackets will depend on whether the operator is bosonic or fermionic. From this operator we can construct its decendants by applying any generator of the superconformal algebra.

An important subset of these primary operators are the *chiral primary operators*, and these are annihilated as in (2.25), and also by at least one Q_α^a,

$$[Q_\alpha^a, O\} = 0. \tag{2.28}$$

Operators of this kind are also known as *BPS* operators. We will next see how these BPS states appear as soliton solutions of Yang-Mills systems.

2.3.4 $\mathcal{N} = 4$ Super Yang-Mills

The field content of $\mathcal{N} = 4$ Super Yang-Mills(SYM) consists of a guage field $A_\mu(x)$, four Weyl fermions $\lambda^a_\alpha(x)$, and six real scalars $\phi^i(x)$, where $a \in \{1,2,3,4\}$, $i \in \{1,2,...,6\}$. The SYM action is,

$$\begin{aligned}\mathcal{L} = \mathrm{Tr}(&-\frac{1}{2g^2_{YM}}F_{\mu\nu}F^{\mu\nu} + \frac{\vartheta}{16\pi^2}F_{\mu\nu}\tilde{F}^{\mu\nu} - i\bar{\lambda}^a\bar{\sigma}^\mu D_\mu\lambda_a \\ &- \sum_i D_\mu\phi^i D^\mu\phi^i + g_{YM}\sum_{a,b,i} C^{ab}_i\lambda_a[\phi^i,\lambda_b] \\ &+ g_{YM}\sum_{a,b,i}\bar{C}_{iab}\bar{\lambda}^a[\phi^i,\bar{\lambda}^b] + \frac{g^2_{YM}}{2}\sum_{i,j}[\phi i,\phi^j]^2),\end{aligned} \tag{2.29}$$

where $F_{\mu\nu}$ is the field strength tensor, D_μ is the covariant derivative, and the C^{ab}_i are the Clebsch-Gordon coefficients.

SYM is scale invariant on the classically, and it also has the rare property that this scale invariance is preserved after quantization, and hence the theory is superconformal. The scale invariance remains at the quantum level as SYM is believed to be UV finite theory, containing no UV divergenes in the loop corrections, or in the corrections to instanton solutions. Also, the β functions vanish at all orders of the perturbation theory.

Another property of the theory that will be useful later, is that it is invariant under the so-called *S-duality* group $SL(2,\mathbb{Z})$. This duality implies a strong-weak duality, for upon acting with the transformation, the coupling constant g_{YM} becomes $\frac{4\pi}{g_{YM}}$.

2.3.5 Superstring theory and supergravity

Starting from bosonic string theory, one obtain superstring theory by adding fermionic degrees of freedom, which is naturally done by introducing supersymmetry. As in bosonic string theory, we find the equations of motion from the supersymmetrized Polyakov actions and we obtain a boundary term which imposes boundary conditions. From these conditions the two type of possible string solutions fall out: open and closed superstrings.
Inside the open superstring sector, one finds there are two possible boundary conditions, corresponeding to the Neveu-Schwarz(NS) and Ramond(R) sectors, which further imply that superstring theories require that $D = 10$, and they also imply that the ground state of the NS sector is tachyonic. In order to remove this tachyon, a truncation prescription known as the *GSO projection*, projects out the tachyons while also leaving an equal number of fermions and bosons, thus realising the supersymmetry of the target spacetime. Within the closed superstring sector, as aresult of the GSO projection, there can exist four different superstring theories in ten dimensions, however the one we are concerned with is known as type IIB superstring theory.

Type IIB supergravity

Taking what is known as the low-energy limit of type II superstring thories, involves taking the string coupling constant to zero, and hence only taking the massless closed superstring states. From these

states one arrives at the low-energy effective action for the superstring theory, known as type IIB supergravity. The bosonic part of the action is as follows,

$$\begin{aligned}\mathcal{S}_{IIB} = \frac{1}{2\bar{\kappa}_{10}^2}[\int \mathrm{d}^{10}X\sqrt{-g}\Big(e^{-2\phi}(R + 4\partial_M\phi\partial^M\phi - \frac{1}{2}|H_{(3)}|^2]) \\ -\frac{1}{2}|F_{(1)}|^2 - \frac{1}{2}|\tilde{F}_{(3)}|^2 - \frac{1}{4}|\tilde{F}_{(5)}|^2 \\ -\frac{1}{2}\int C_{(4)} \wedge H_{(3)} \wedge F_{(3)}],\end{aligned} \tag{2.30}$$

whereκ_{10}^2 is the ten dimensional gravitational constant, and the field strength tensors are given by the following,

$$\begin{aligned}F_{(p)} = \mathrm{d}C_{(p-1)}, H_{(3)} = \mathrm{d}B_{(2)}, \tilde{F}_{(3)} = F_{(3)} - C_{(0)}H_{(3)}, \\ \tilde{F}_{(5)} = F_{(5)} - \frac{1}{2}C_{(2)\,(3)} + \frac{1}{2}B_{(2)\,(3)},\end{aligned} \tag{2.31}$$

where d is the exterior derivative and F is self-dual.

This theory is chiral and violates parity, which can be seen in its field content:

$$\begin{aligned}&\bullet\ g_{MN} \rightarrow \text{metric/graviton},\\ &\bullet\ C_{(0)} + ie^{-\phi} \rightarrow \text{axion-dilaton},\\ &\bullet\ B_{(2)}, C_{(2)} \rightarrow \text{two-forms},\\ &\bullet\ C_{(4)} \rightarrow \text{self-dual four-form},\\ &\bullet\ \Psi_{I\alpha}^M, I = 1,2 \rightarrow \text{Majorana-Weyl gravitinos},\\ &\bullet\ \lambda_{I\alpha}, I = 1,2 \rightarrow \text{Majorana-Weyl dilatinos}.\end{aligned} \tag{2.32}$$

Type IIB supergravity possesses a duality useful to us: S-duality. This is the same duality as introduced in the previous section, a mapping between a weakly coupled superstring theory and a strongly coupled superstring theory. In this case it is a mapping from type IIB supergravity to itself.

2.3.6 D-branes

Now we will look at the non-perturbative objects in the theory, known as D-branes. These objects arise from the boundary conditions of open strings, where in particular they are the hypersurfaces on which open strings can end. The open string lead then to masless excitations on the D-branes; scalars and a U(1) gauge field A_μ, which show us that the brane is in fact a dynamical object.

D-branes can also be viewed in an alternative way however; they can be seen as massive, gravitating objects, due to their coupling to the closed strings in the NS-NS sector. This come from the fact that extremal *p-branes*, which are solition solutions in supergravity, are equivalent to D-branes. Due to their boundary conditions, D-branes break one half of the supercharges of the background, and hence carry the same charge as the p-branes. Therefore, we can view these as two descriptions of the same object, and we can consider Dp-branes to be BPS solutions to the supergravity equations of motion.

It will be useful to look at what this means for 10-dimensional type IIB supergravity. The following ansatz solves the equations of motion,

$$\begin{aligned} ds^2 &= H_p(r)^{\frac{1}{2}}\eta_{\mu\nu}da^\mu dx^\nu + H_p(r)^{\frac{1}{2}}dy^i dy^i, \\ e^\phi &= g_s H_p(r)^{\frac{(3-p)}{4}}, \\ C_{(p+1)} &= \left(H_p(r)^{-1} - 1\right) dx^0 \wedge dx^1 \wedge ... \wedge dx^p, \\ B_{MN} &= 0, \end{aligned} \tag{2.33}$$

where x^μ, $\mu = 0, 1, ..., p$ are the coordinates on the brane worldvolume, and y^i, $i = p+1, ..., 9$ are the coordinates perpendicular to the Dp-brane. Also, r is defined as $r^2 = \sum_{p+1}^{9} y_i^2$. Plugging this ansatz into the equations of motion imposes a restriction on the function $H_p(r)$, namely that

$$\Box H_p(r) = 0, \tag{2.34}$$

so now we know that $H_p(r)$ is a harmonic function, and can hence be written as,

$$H_p(r) = 1 + \left(\frac{L_p}{r}\right)^{(7-p)}. \tag{2.35}$$

To determine L_p, we need to find the charge of the Dp-brane, which can be can be found as follows,

$$Q = \frac{1}{2k_{10}^2}\int_{S^{8-p}} *F_{p+2}, \tag{2.36}$$

where $*$ is the ten dimensional Hodge operator. For this setup, Q is found to be $Q = N \cdot \mu_p$. Now if one sets $Q = N$ and evaluates the integral in 2.36 L_p is found to be,

$$L_p^{7-p} = (4\pi)^{\frac{(5-p)}{2}}\Gamma\left(\frac{7-p}{2}\right) g_s N \alpha'^{\frac{(7-p)}{2}}. \tag{2.37}$$

In the case of D3-branes, which will be useful later, L_p is found to be,

$$L_3^4 = 4\pi g_s N \alpha'^2 \tag{2.38}$$

The two visualizations of D-branes will play in important role in the correspondence so it is worth detailing them and their consequences once more. The alternative views can be seen as the different perspectives open and closed strings have for the D-branes. For the open strings, D-branes are hypersurfaces on which they terminate.

The open strings in this picture are small perturbations to the D-brane, and hence we can only treat this view as reliable if the string coupling constant is very small, i.e. $g_s \ll 1$. If we then take the low energy limit, only massless states remain and the dynamics of the open strings are that of a supersymmetric gauge theory on the worldvolume of the D-brane. If we now consider N coincident D3-branes, we know that the gauge group of such a system is $U(N)$, and hence the effective coupling constant is $g_s N$. This then tells us that this perspective is only valid for $g_s N \ll 1$.

The closed string on the other hand, sees the D-brane as a massive object, being a solition solution of supergravity. In order for the supergravity solution to be valid, the curvature must be small and so the charach=teristic lengthscale L should be large. If we have N coincident D-branes, from 2.37 we see that $\frac{L^4}{\alpha'^2} \propto g_s N$, and so for this perspective of the D-brane to be valid, $g_s N \gg 1$.

We will see in the next section that when we look at N coincident D3-branes through these perspectives we can motivate the correspondence.

2.4 AdS/CFT correspondence

We are now ready to motivate the argument for the AdS/CFT correspondence, as done by Maldacena. As stated, in its simplest form it relates type IIB superstring theory compactified on $AdS_5 \times S^5$, and $\mathcal{N} = 4$ Super Yang-Mills theory in $3+1$ dimensions. It is now clear that there exists a dual perspective on D-branes, depending on if you are an open or closed string, and it is this identification that allows one to motivate the correspondence.

To begin, we will start with the **open string perspective**, valid in the $g_s N \ll 1$, weakly coupled regime. Consider type IIB superstring theory in flat $(9+1)$-dimensional Minkowski spacetime, where N coincident D3-branes are embedded. It should be noted that this setup breaks one half of the supercharges of the background. The string theory on this background contains two kinds of perturbative excitations; open strings and closed strings. The open strings correspond to excitations of the D-branes and closed strings correspond to excitations of the empty space.

If one considers the system at low energies (i.e. those less than the string scale $\frac{1}{l_s}$), only the massless states of the spectrum remain and they form a supermultiplet. The closed string states form a ten dimensional $\mathcal{N} = 1$ supermultiplet, and the open string states form a four dimensional $\mathcal{N} = 4$ supermultiplet, which consists of a gauge field and six real scalar fields. The effect action for the massless states can be written as,

$$S = S_{\text{open}} + S_{\text{closed}} + S_{\text{int}}, \tag{2.39}$$

where S_{int} is the action for the interactions between open and closed string states. The actions are as follows,

$$\begin{aligned} S_{\text{closed}} &= \frac{1}{2\kappa^2} \int d^{10}x \sqrt{-g} e^{-2\phi} \left(R + 4\partial_M \phi \partial^M \phi) \right) + ... \\ S_{\text{open}} &= -\frac{1}{2\pi g_s} \int d^4x \left(\frac{1}{4} F_{\mu\nu} F^{\mu\nu} + \frac{1}{2} \eta^{\mu\nu} \partial_\mu \phi^i \partial_\nu \phi^i + O(\alpha') \right), + ..., \\ S_{\text{int}} &= -\frac{1}{8\pi g_s} \int d^4x \phi F_{\mu\nu} F^{\mu\nu}, \end{aligned} \tag{2.40}$$

where κ is given by $2\kappa^2 = (2\pi)^7 \alpha'^4 g_s^2$, and g_{MN} and ϕ are the metric and dilaton respectivly.

If we generalise S_{open} and S_{int} to N D3-branes, the gauge group of the gauge fields and scalar field is $U(N)$, and the trace needs to be taken over the kinetic terms. Partial derivatives will become covariant derivatives and a scalar potential will be added to the action. If one now takes the low energy limit, $\alpha' \to 0$, then S_{open} reduces to the bosonic part of $\mathcal{N} = 4$ Super Yang-Mills theory, provided one identifies,

$$2\pi g_s = g_{YM}^2. \tag{2.41}$$

Furthemore, in this limit S_{closed} reduces to that of supergravity in $(9+1)$-dimensional Minkowski spacetime, and S_{int} vanishes, implying that the open and closed string states decouple.

Next we consider the **closed string perspective**, where we are in the $g_s N \gg 1$, strongly coupled regime. In this view the N D3-branes are solutions to the supergravity equations of motion preserving the $SO(3,1) \times SO(6)$ isometries of $\mathbb{R}^{9,1}$, and 16 of the 32 supercharges of type IIB supergravity. This solution is given by,

$$\begin{aligned} ds^2 &= H(r)^{-\frac{1}{2}} \eta_{\mu\nu} dx^\mu dx^\nu + H(r)^{\frac{1}{2}} \delta_{ij} dx^i dx^j, \\ e^{2\phi(r)} &= g_s^2, \\ C_{(4)} &= (1 - H(r)^{-1}) dx^0 \wedge dx^1 \wedge dx^2 \wedge ..., \end{aligned} \tag{2.42}$$

where $\mu, \nu = 0, 1, 2, 3$ and $i, j = 4, 5, ..., 9$, and the radial coordinate is defined by $r^2 = \sum_{i=4}^{9} x_i^2$. The ... in the expression for $C_{(4)}$ represents terms which do not contribute to what follows.

Inserting the ansatz into the type IIB equations of motion one finds that $H(r)$ is a harmonic function obeying $\Box H(r) = 0$, which implies that,

$$H(r) = 1 + \left(\frac{L}{r}\right)^4. \tag{2.43}$$

Using the same argument that lead to 2.37, we can deduce that

$$L^4 = 4\pi g_s N \alpha'^2. \tag{2.44}$$

Clearly the value of $H(r)$ will change considerably depending on what region we consider, i.e. $r \gg L$ where $H(r) \sim 1$, or $r \ll L$ where $H(r) \sim \frac{L^4}{r^4}$. In the first case, taking that ansatz for L results in the metric 2.42 reducing to ten dimensional flat spacetime. In the second case, known as the *near-horizon region*, the metric becomes,

$$\begin{aligned} ds^2 &= \frac{r^2}{L^2}\eta_{\mu\nu}dx^\mu dx^\nu + \frac{L^2}{r^2}\delta_{ij}dx^i dx^j \\ &= \frac{L^2}{z^2}\left(\eta_{\mu\nu}dx^\mu dx^\nu + dz^2\right) + L^2 ds^2_{S^5}, \end{aligned} \tag{2.45}$$

where the new coordinate $z = \frac{L^2}{r}$, as well as spherical coordinates $\delta_{ij}dx^i dx^j = dr^2 + ds^2_{S^5}$, were introduced. In the second line, we see that the geometry of the near horizon region is $AdS_5 \times S^5$

Taking the low energy limit, it is found that again the closed and open string states decouple. As a result we are left with two distinct perspectives of closed strings at low energy: supergravity modes in ten dimensional flat spacetime, and string excitations in near-horizon region which has the geometry of $AdS_5 \times S^5$ spacetime. So in one case we have type IIB supergravity in ten dimensional spacetime, and in the other we have fluctuations about $AdS_5 \times S^5$ spacetime solution of type IIB supergravity.

Now we are ready to present the correspondence, and all that needs to be done is to combine these perspectives of open and closed strings, which we said should be equivalent. After taking the low energy limit we were left with the following perspectives,

Closed string perspective	**Open string perspective**
type IIB supergravity on $AdS_5 \times S^5$	$\mathcal{N} = 4$ Super Yang-Mills on flat 4D spacetime
type IIB supergravity on $\mathbb{R}^{9,1}$	type IIB supergravity on $\mathbb{R}^{9,1}$

Since these two points of view are equivalent, and type IIB supergravity on $\mathbb{R}^{9,1}$ is appearing on both sides, we are led to identify type IIB supergravity on $AdS_5 \times S^5$ and $\mathcal{N} = 4$ Super Yang-Mills on flat 4D spacetime in order to maintain the equivalence. Here is where Maldacena made his conjecture, that this all implies that type IIB supergravity on $AdS_5 \times S^5$ and $\mathcal{N} = 4$ Super Yang-Mills on flat 4D spacetime are dynamically equivalent.

So now we have the AdS/CFT correspondence as Maldacena laid out, and this one is what is known as the *weak form* of the correspondence. There exists however a stronger form of the corespondence , adeptly called the *strongest form* as it works for any values of N and λ, where $\lambda = g^2_{YM}N$. This means that we can take any g_s, and so the string theory involved is a quantum string theory. This is usually too restrictive for performing calculations, so it is useful to lessen the conditions by taking certain limits. Lessening the restrictions a bit more, we arrrive at the *strong form* of the correspondence, where we take $g_s \to 0$ while keeping $\frac{L}{\sqrt{\alpha'}}$ constant. One can understand why this limit is useful, as it amounts to considering $g_s \ll 1$, so weak coupling in the string theory, and this means we can perform perturbation

theory, which is the regime in which string theory is presently best understood. In this limit $g_s \to 0$, the theory is at leading order and so reduces to being a classical string theory. Looking at 2.44 and 2.41, the correspondence then tells us that on the CFT side this limit means that $g_{YM} \ll 1$, while λ must stay fixed but arbitrary. As a result, we must take $N \to \infty$ in order for this condition to hold, and so we are considering a gauge theory in the 't Hooft limit (large N at fixed λ). Therefore it is now clear that AdS/CFT is a realisation of 't Hooft's idea that in this limit a gauge theory is equivalent to a string theory. Finally then we have the weak form of the correspondence, which we use when we want to study strongly coupled field theories. As we saw, this is done by taking the limit $\lambda \to 0$, which on the other side of the correspondence amounts to taking $\frac{\alpha'}{L^2} \to 0$ and $g_s \to 0$. Which turned out to be the limit of classical supergravity, and so we see the correspondence as a mapping between stringly coupled $\mathcal{N} = 4$ Super Yang-Mills and weakly curved $AdS_5 \times S^5$.

2.4.1 Field-Operator Map

The AdS/CFT correspondence naturally leads to a correspondence mapping between the fields and operators associated with the AdS and CFT sides respectively. This happens because the symmetries, namely the $PSU(2,2 \mid 4)$ symmetry, of both sides are the same, and so the fields and operators will live in the same representations. Performing a Kaluza-Klein reduction on the supergravity fields, these fields and the relavent operators on the field theory side will be in the same representation if one identifies $l = \Delta$, where l is the rank of the symmetric traceless tensor defining the spherical harmonics,

$$Y^I = C^I_{i_1 \ldots i_l} x^i \ldots x^l, \tag{2.46}$$

and Δ is the conformal dimension of the primary operators.

These identifications lead to the following relations, in $d-$dimensions, between the mass m, of the supergravity field and Δ,

- scalars and massive spin two fields $\to m^2L^2 = \Delta(\Delta - d)$,
- massless spin two fields $\to m^2L^2 = 0, \Delta = d$,
- p-form fields $\to m^2L^2 = (\Delta - p)(\Delta + p - d)$,
- spin$\frac{1}{2}, \frac{3}{2} \to |m|L = \Delta - \frac{d}{2}$,
- rank s symmetric traceless tensor $\to m^2L^2 = (\Delta + s - 2)(\Delta - s + 2 - d)$.

This relationship can be further exemplified if one considers the boundary behaviour of the supergravity fields. Co We know from string theory that the coupling constant is related to the expectation value of the dilaton field, $g_s = e^{\Phi(X)}$, and this expectation value is set by the boundary behaviour of the dilaton, therefore we see that changing the coupling constant of the string results in a change in the boundary value of the dilaton.

Consider a scalar field ϕ, dual to some primary operator, and take the toy model action

$$S = \frac{-C}{2} \int dz d^d x \sqrt{-g} (g^{mn} \partial_m \phi \partial_n \phi + m^2 \phi^2). \tag{2.47}$$

It is convienent to use AdS Poincaré patch coordinates where the metric is given by,

$$ds^2 = \frac{L^2}{z^2} \left(dz^2 + \eta_{\mu\nu} dx^\mu dx^\nu \right), \tag{2.48}$$

and it will also be helpful to decompose the x^μ directions into their Fourier modes and consider plane wave solutions of the form $\phi(z,x) = e^{ip^\mu x_\mu} \phi_p(z)$. Solving the Klein-Gordon equation for the modes

$\phi_p(z)$ results in two solutions, whose asymptotic behaviour ($z \to 0$) is as follows,

$$\phi_p^1(z) \sim z^{\Delta_+}, \quad \phi_p^2(z) \sim z^{\Delta_-}, \tag{2.49}$$

where $\Delta_\pm$ is given by

$$\Delta_\pm = \frac{d}{2} \pm \sqrt{\frac{d^2}{4} + m^2 L^2}. \tag{2.50}$$

$\phi_p^1(z)$ is a normalisable solution, whereas $\phi_p^1(z)$ is non-normalisable, where normalisable means that the action is finite when evaluated on the solution. The scalar field can then be expanded around the boundary ($z \to 0$) as,

$$\phi(z,x) \sim \phi_{(0)}(x) z^{\Delta_-} + \phi_{(+)} z^{\Delta_+} + ... \tag{2.51}$$

Dimensional analysis then shows that ϕ_+ is the vacuum expectation value of the dual operator of dimension Δ_+, and $\phi_{(0)}$ is the source for this operator.

This relationship between the boundary value of the supergravity field and the field theory operator O, implies that there is a duality between the generating functionals of both theories. It was presented by Gubser, Klebanov, and Polyakov in [7], and Witten in [8] that the generating functional of correlators on the field theory side is related to the partition function of string theory by,

$$\langle e^{\int d^d x \phi_{(0)}(x) O(x)} \rangle_{CFT} = \mathcal{Z}_{\text{string}}[\phi(z,x)|_{z=0} = \phi_{(0)}(x)] \tag{2.52}$$

This form of the correspondence presents us with a method to calculate the correlation functions of the operators on the field theory side; once we know the bulk field ϕ that is dual to the operator O in question, we compute the supergravity action and solve the equations of motion subject the the boundary condition $\phi(z,x) \sim z^{\Delta_-}\phi_{(0)}(x)$ as $z \to 0$. Then, this solution is put into the supergravity action, and we take the functional derivatives with respect to the source $\phi_{(0)}$ to retrieve the correlation functions.

Chapter 3

Applied AdS/CFT methodologies

Now we have all the basics of the correspondence, and we can suitably build upon them in order to get what is needed in the context of this thesis. We are concerned with a strongly interacting condensed matter system undergoing a phase transition, at finite chemical potential χ and magnetic field B. These ensembles will deform the theory, so in this chapter these deformations will be outlined, and the consequences will be discussed.

3.1 Finite temperature at equilibrium

It is expected that the above quantities should break the scale invariance of the spacetime. If we take AdS spacetime in the following coordinates,

$$ds^2 = \frac{L^2}{r^2}\left(-dt^2 + dr^2 + dx^i dx^i\right), \tag{3.1}$$

the scale invariance can be broken while preserving rotation and translation invariance if one adds non-trivial radial functions to the metric,

$$ds^2 = \frac{L^2}{r^2}\left(-f(r)dt^2 + g(r)dr^2 + h(r)dx^i dx^i\right), \tag{3.2}$$

and these functions can be determined from the equations of motion of the system in consideration. If $f(r) \neq h(r)$, Lorentz invariance is also broken, which is also to be expected. At high energies, the scale invariance should be recovered, and so as we appraoch the boundary where the CFT lives, we should impose that the radial functions behave as,

$$f(r), g(r), h(r) \to \text{const.} \quad \text{as} \quad r \to 0, \tag{3.3}$$

thus, recovering the AdS spacetime metric. It can be shown [9], [1] that horizons correspond to thermally mixed states in the field theory. In essence, one finds that in order for the spacetime to remain regular at the horizon, the Euclidian time must be periodically identified. This will then have implications for the dual field theory; the temporal direction of the field theory is also periodically identified, and it is known that such a constraint entails that we are considering the field theory at finite temperature and equilibrium, the temperature given by the inverse of the periodicity.

For example, consider the analytically continued Schwarzschild-AdS metric,

$$ds^2 = \frac{L^2}{r^2}\left(f(r)d\tau^2 + \frac{dr^2}{f(r)} + dx^i dx^i\right), \tag{3.4}$$

Since $f(r)$ vanishes at the horizon (r_+), we must impose the periodicity condition on the τ coordinate in order for g_{rr} to remain finite,

$$\tau \sim \tau + \frac{4\pi}{|f'(r_+|}. \tag{3.5}$$

To see what this means for the field theory, we need to determine the background metric, which can be found from the boundary behaviour of metric,

$$g_{\mu\nu}(r) = \frac{L^2}{r^2} g_{(0)\mu\nu} + \cdots \quad \text{as} \quad r \to 0. \tag{3.6}$$

$g_{(0)\mu\nu}$ can be interpreted as being the background metric, which we can see is given by $ds^2 = d\tau^2 + dx^i dx^i$. τ is still periodically identified, and hence we know that the field theory in question is at finite temperature,

$$T = \frac{d}{4\pi r_+}. \tag{3.7}$$

In essence, we see that a planar black hole is dual to a finite temperature. So in order to add thermodynamics to the field theory, one just has to add a black hole to the gravity side, and it is then possible to calculate the desired thermodynamic quantities such as the free energy and entropy.

3.2 Finite chemical potential and magnetic field at equilibrium

Our condensed matter system contains an electromagnetic $U(1)$ symmetry, so we want to figure out what the dual of this is. First of all, we should make it clear that this symmetry can be considered as a *global* $U(1)$ symmetry. This is because in these condensed matter systems, it is possible to write down an effective field theory that contains no gauge bosons, but does involve charged fields, and so we take this symmetry as no longer being gauged.

It turns out that the AdS/CFT correspondence also provides us with another duality; one between global symmetries at the boundary (field theory) and gauge symmetries in the bulk (AdS) This can be understood by considering the following; near the boundary ($r \to 0$) the energy scale should be vanishing since it will completely vanish in the CFT ($r = 0$), but deep in the bulk spacetime ($r \to \infty$) there will be an associated energy scale. So in a sense, the radial coordinate r, can be thought of as a geometric representation of the energy scale. The field theory is globally invariant under conformal transformations, in the bulk spacetime however, these symmetries are no longer global. Instead, we see that the radial coordinate transforms under the scale transformation, and this combined with the other coordinate scale transformations are the isometries of the bulk spacetime metric,

$$\begin{aligned} x^\mu \to \lambda, x^\mu \quad r \to \frac{r}{\lambda}, \\ ds^2 = \frac{L^2}{r^2} dr^2 + \frac{r^2}{L^2} (\eta_{\mu\nu} dx^\mu dx^\nu). \end{aligned} \tag{3.8}$$

Finally, we know that these isometries of the metric are exactly the diffeomorphisms of general relativity, which are of course gauge transformations. It is also worth noting what may have become obvious now, that the energy scale in the bulk gives us a clear representation of the UV and IR behaviour of the field theory, i.e. that near the boundary we have the UV regime and deep in the bulk we have the IR regime.

$$\begin{array}{ccc} \text{Global symmetry (field theory)} & \Longleftrightarrow & \text{Gauge symmetry (gravity)} \\ d \text{ spacetime dimensions} & & d+1 \text{ spacetime dimensions} \end{array}$$

So from all this we gather that this $U(1)$ global symmetry is dual to a gauge symmetry in the bulk, and in that case to achieve this setup one must add a Maxwell field to the bulk spacetime. For example one could arrive at the Einstein-Maxwell action,

$$S_{\text{EM}} = \int d^{d+1}x \sqrt{-g} \left[\frac{1}{2\kappa^2} \left(R + \frac{d(d-1)}{L^2} \right) - \frac{1}{4g^2} F^2 \right], \tag{3.9}$$

where $F = dA$ is the electromagnetic field strength.

While preserving rotational symmetry, the chemical potential $\mu = A_{(0)t}$, and magnetic field $B = F_{(0)xy}$ can be introduced. Note though that the magnetic field is rotationally invariant in $2+1$ dimensions only. These are found from the boundary value of the bulk Maxwell field,

$$A_\mu = A_{(0)\mu} + \cdots . \tag{3.10}$$

Consequently, when considering now the effect of the the $U(1)$ global symmetry we must consider the metric 3.2 together with a non-vanishing Maxwell field in the bulk,

$$A = A_t(r)dt + B(r)xdy. \tag{3.11}$$

From here, one can compute quantities such as the thermodynamic potential, charge density, and magnetisation density. It is also possible to compute the temperature as before. In our case, since we are working in $d = 3$, the rotational symmetry is preserved, if we were in higher dimensions the magnetic field would break this symmetry.

3.3 Quasinormal modes

We have seen in the previous chapters that there exists a duality between thermal quantum field theories in equilibrium and planar black holes, so it is a natural expectation that if one perturbs the black hole solution it amounts to fluctuations around thermal equilibrium in the field theory. In order to explore this further we need to first understand the dynamics of these perturbations, which we will now see is governed by the quasinormal modes of the system.

Quasinormal modes are the eigenmodes of dissiapative systems; the perturbations are damped, and decay in a way similar to how the ringing of a bell subsides, namely the process is characterised by an exponential decay of the form $e^{-i\omega t}$, where ω is a complex frequency. Perturbations around black hole solutions naturally lead to quasinormal modes, since the fluctuations produced can fall back into the black hole and are therefore decaying. Similar to the bell, the quasinormal modes are the 'ringing' of a black hole returning to equilibrium. Theoretical discoveries such as black-hole radiation [5], and its associated radiation and temperature [6], suggests that black holes behave as thermodynamic systems in many ways. It was shown in [10] that there exists a universal bound on the relaxation time of perturbed thermodynamic systems,

$$\tau_{\text{min}} = \frac{\hbar}{\pi T}, \tag{3.12}$$

where k_{B} has been set to one.

The relaxation time for the perturbations to cease can be determined from the quasinormal modes, namely from the imaginary part of the quasinormal mode frequencies. These are inversely proportional to each other $\tau^{-1} \equiv \text{Img}(\omega_0) \equiv \omega_{\text{I}}$, so there are an infinite number of quasinormal frequencies, with decreasing relaxation time. Consequently, the mode with the smallest imaginary part, also known as the fundamental mode, has the longest relaxation time, and determines the characteristic timescale for generic perturbations to decay. Considering this, one can see that 3.12 becomes a bound on the fundamental mode,

$$\omega_{\text{I}} \leq \frac{\pi T}{\hbar}, \tag{3.13}$$

and in this way we see that the black hole must have at least one mode which satisfies this bound, and this mode will be the longest living one, determining the characteristic timescale for the dynamics. The bond is satisfied for any physical system that exhibits hydrodynamic behaviour, since there are always modes that are sufficiently long lived [11], and we will make use of this feature later when determining

the boundary of the quantum critical region.

The quasinormal modes of a given field (scalar, gauge, etc.) can be found on the gravity side by solving the fluctuation equation for said field about the gravity background, subject to infalling boundary conditions at the horizon. It should be noted that the other boundary condition, that at spatial infinity, depends on the spacetime one is considering. For anti-de Sitter spacetimes, the condition at the conformal boundary is not obvious; if scalar field fluctuations are being considered, choosing Dirichlet boundary conditions at spatial infinity ensures that the quasinormal modes coincide with the singularities of the retarded Green's function in the dual theory.

Electromagnetic and gravitational fluctuations are often more interesting to consider as they couple to conserved symmetry currents in the dual field theory, however the choice of boundary conditions at spatial infinity is not so obvious. A convenient approach is to construct gauge invariant combinations of the fluctuations, and impose the Dirichlet boundary conditions on these combinations. This ensures that the resulting quasinormal modes correspond to the poles of the gauge theory correlation function, this purpose being discussed in a moment.

Using the gauge/gravity duality recipe for constructing the field theory correlators, one finds a very important and useful result: the quasinormal mode spectra of a black hole corresponds to the poles of the retarded Green's functions in the field theory. To see this consider a scalar perturbation, recall that the solution on the boundary ($r \to \infty$) can be written as,

$$\delta\phi(r,\omega,q) = \mathcal{A}(\omega,q)r^{-\Delta_-} + \mathcal{B}(\omega,q)r^{\Delta_+} + \cdots \tag{3.14}$$

where Δ_- and Δ_+ are the non-normalisable and normalisable solutions respectively.

Using the duality perscription, the Minkowski space correlators can be found, and in particular the retarded two-point function is found to be,

$$G^{\mathrm{R}}(\omega,q) \sim \frac{\mathcal{B}}{\mathcal{A}} + \text{contact terms}, \tag{3.15}$$

and so we see that the poles of the correlator are just given by the zeros of $\mathcal{A}(\omega,q)$. However, from the gravity point of view, the condition $\mathcal{A}(\omega,q) = 0$ is just the Dirichlet boundary condition that defines the quasinormal modes.

For example in [12] they compute the retarded correlators for a $2D$ CFT, dual to a BTZ black hole. The retarded two-point function of the operator of conformal dimension $\Delta = 2$ is given by

$$G^{\mathrm{R}} \sim \frac{\omega^2 - q^2}{4\pi^2}\left[\psi\left(1 - i\frac{\omega - q}{4\pi T}\right) + \psi\left(1 - i\frac{\omega + q}{4\pi T}\right)\right], \tag{3.16}$$

where $\psi = \frac{\Gamma'(z)}{\Gamma(z)}$, and the constant prefactor is left out for simplicity. It can be observed that the correlator has infinitely many poles in the complex frequency plane located at,

$$\omega_n = \pm q - 4i\pi T(n+1), \quad n = 0, 1, 2, \ldots \tag{3.17}$$

and these are precisely the quasinormal mode frequencies.

Hence, we see that all the information about the poles of the correlators is contained within in the quasinormal modes spectrum. From this one can determine useful information about the gauge theory, such as the particle spectrum and transport coefficients.

Another important and more relevant consequence of the duality arises as follows. The correspondence tells us that that black holes are dual to thermal states in the field theory, therefore we can imagine

if we were to perturb the black hole solution if would amount to perturbing the thermal state out of thermal equilbrium. Quasinormal modes are simply the perturbations of the black hole, and we know that we can find the characteristic timescale for the perturbations to decay from the fundamental mode. The correspondence then says that this timescale is exactly the equilibration time for the thermal state, i.e. the time it takes for the thermal state to return to thermal equilibrium.

$$\begin{array}{ccc} \text{characteristic decay timescale} & \Longleftrightarrow & \text{equilibration timscale} \\ \text{(black hole)} & & \text{(thermal state)} \end{array}$$

We will see later how this will be very imporant for us to be able to determine the boundary of the quantum critical region.

3.3.1 Example: A massless scalar in AdS_5

In this thesis, a Mathematica package created in [13] will be used to compute the quasinormal modes, and here we reproduce a simple example of an application of the code to a massless scalar field.

The method of numerical computation requires that the equations be written in Eddington-Finklestein coordinates. In these coordinates, the infalling boundary conditions become a requirement that the fluctuation be regular at the horizon. The metric in these coordinates is given by ,

$$ds^2 = -f(r)dt^2 + 2drdt + r^2 d\mathbf{x}^2, \tag{3.18}$$

where $f(r) = r^2(1 - r^{-4})$, and so the horizon is at $r = 1$ and the boundary at $r \to \infty$. Since we are always interested in the boundary asymptotics, it will be more useful to change coordinates $u = \frac{1}{r}$, so that the boundary is now at $u = 0$. Now the metric reads,

$$ds^2 = -f(u)dt^2 - \frac{2}{u^2}dudt + \frac{1}{u^2}d\bar{x}^2, \tag{3.19}$$

where $f(u) = u^{-2}(1 - u^4)$.

We are looking at scalar perturbations, so we take the massless scalar action below which gives the following equation of motion,

$$\begin{aligned} S &= -\frac{1}{2}\int d^5x \partial_\mu\phi\partial^\mu\phi, \\ \partial_\mu &\left(g^{\mu\nu}\sqrt{-g}\partial_\nu\phi\right) = 0. \end{aligned} \tag{3.20}$$

Choosing a plane wave ansatz for the scalar perturbations,

$$\delta\phi(x,t,u) = \delta\phi(u)e^{-i(\omega t - kx)}, \tag{3.21}$$

the following equation of motion for $\delta\phi$ is obtained,

$$(u - u^5)\delta\phi''(u) + (4i\lambda - u^4 - 3)\delta\phi'(u) - (4q^2u + 6i\lambda) = 0, \tag{3.22}$$

where ω and k have been rescaled, creating the dimensionless quantities $\lambda = \frac{\omega}{2\pi T}$ and $q = \frac{k}{2\pi T}$, where T is the temperature of the black hole. It should also be noted that the equation is linear in ω, and this is a consequence of choosing the Eddington-Finklestein coordinates.

Next, the boundary behaviour of the field must be analysed, so that the appropriate boundary conditions can be imposed. Taking the ansatz $\delta\phi(u) \propto u^p$, one finds that there are two solutions, $\delta\phi \propto 1$ and $\delta\phi \propto u^4$. The first solution is non-normalisable, so it is discarded. Keeping the second solution, it must be rescaled by $\delta\phi(u) = u^3\delta\tilde{\phi}(u)$, such that the solution approaches zero linearily at the boundary. Finally, a further rescaling of the fluctuation equation must be done in order for the equation to tend to

a non-trivial constant on the boundary. Doing this, the following equation is found,

$$(u^2 - u^6)\delta\tilde{\phi}''(u) + u(3 - 7u^4 + 4iu\lambda)\delta\tilde{\phi}'(u) - (3 + 9u^4 + 4q^2u^2 - 6iu\lambda)\delta\tilde{\phi}(u) = 0. \tag{3.23}$$

Once this fluctuation equation is obtained in this correct form, the code can easily be implemented, (DISCUSS IN APPENDIX) and the modes can be found. Below is a plot of the modes calcuated using the most basic function GetModes[eq,40,0], which calculates the modes using a discretization method involving discretizing the fluctuation equation (eq) on a grid of 41 points, at machine precision.

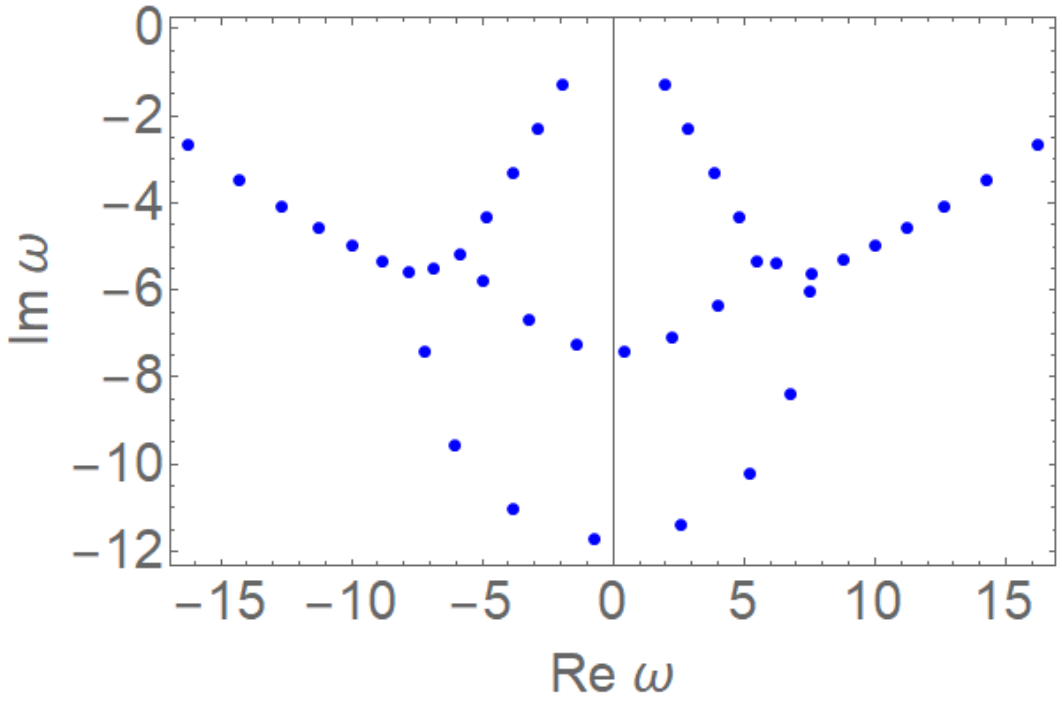

FIGURE 3.1: Modes found using GetModes. Not all of these are modes though, some are numerical artifacts, which need to be removed.

The modes displayed in figure 3.1 are not all actual quasinormal modes, as the modes should lie in an approximate straight line. Some are just numerical artifacts, so in order to remove the artifacts, one must perform the computation at different grid sizes and precisions, compare the results and look for convergence of the modes. This is done by another function, GetAccurateModes[eq,40,0,80,40], which performs the computation first with 41 grid points at machine precision, and then with 81 grid points and precision 40, and it keeps the modes that appear in both computations. Below is a plot of the modes found using this function,

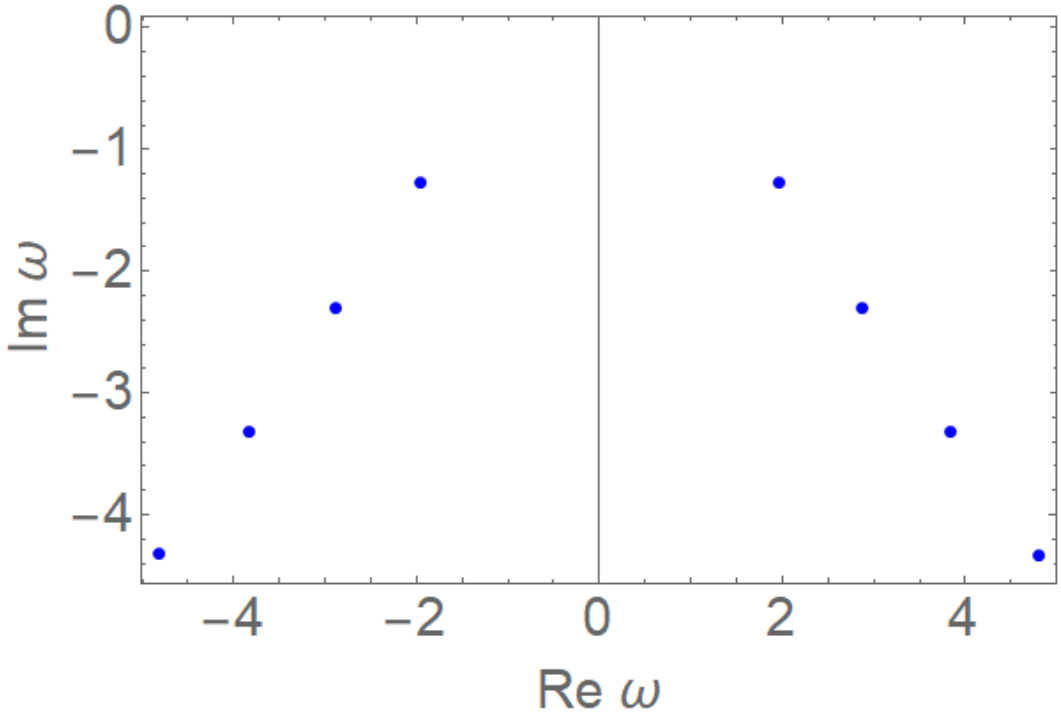

FIGURE 3.2: Modes found using GetAccurateModes. The expected dispersion of modes is observed.

Clearly this method is far more accurate, and it will be principle one employed here. It is also possible to select particular modes and display their values, all of which will be very important to the goal of this thesis.

With this computational method at hand we are now ready to tackle the main goals of this thesis, which will be the topic of the next chapter. Before finishing this chapter however, one final thing should be mentioned, namely one other use of the quasinormal modes to the goals of the thesis; the determination of the quantum critical region of the quantum phase transition.

As stated earlier, the imaginary component of the lowest quasinormal mode is inversely proportional to the characteristic timescale of decay of the black hole/brane perturbations. Using this fact, one can develop an equation that determines the boundary of the quantum critical region of the phase diagram. Recall that the phase diagram is divided into two main regions defined by the relationship between the ground state energy and thermal energy, as shown in figure 3.3.

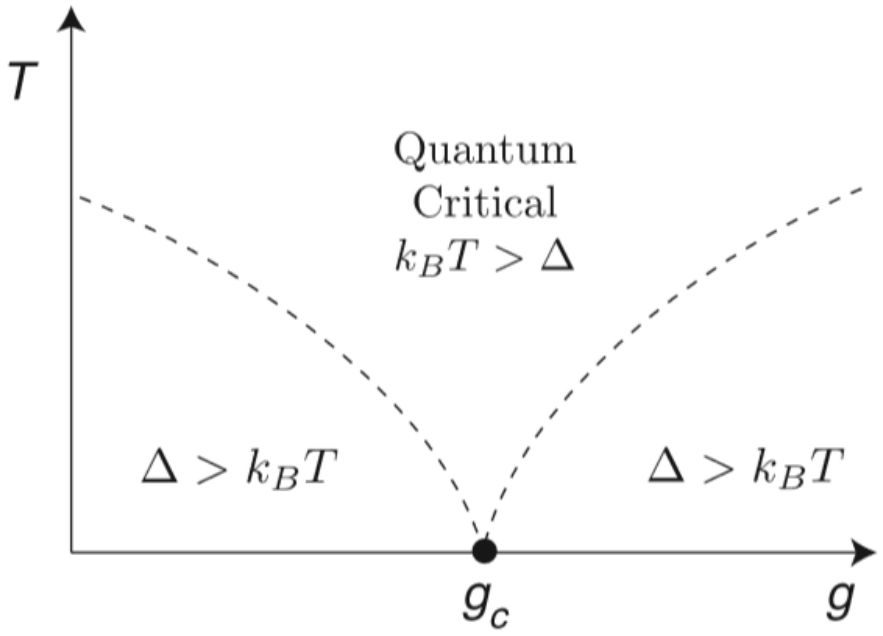

FIGURE 3.3: Typical phase diagram for a quantum phase transition. The different regimes are separated by the quantum critical point which happens at $T = 0$.

Dividing these regions is the boundary of the quantum critical region, which is given by $\Delta = k_B T$. From our discussion about the quasinormal modes, we know that the fundamental mode is equal to the characteristic timescale for the perturbations, and from the AdS/CFT correspondence we know that this is directly equal to the equilibration time for the thermal field theory. Lastly, we know that in the quantum critical region $\tau_{eq} \sim \frac{1}{k_B T}$, and so we can rewrite the boundary equation in terms of the fundamental mode, The equation then becomes

$$|\omega_I| = \Delta. \tag{3.24}$$

It should be noted however that this equation is more of a rough estimation for where the boundary is, as we are dealing with proportionalities. It should be sufficient enough to give us the approximate location of the boundary however. In order to determine the quantum critical region all we must do is find the equation and use it to plot the phase diagram, which in our case will be a $T - B$ phase diagram, where B the magnetic field is the parameter with which the phase transition is controlled by. As we will see later, this will require us to use this equation to determine $b(B)$ and put this into our equation for the temperature.

Chapter 4

The problem and investigation

The task of this thesis is to further the analysis of the following paper [14], which investigates a magnetically induced quantum critical point in holography. It is first necessary to describe the setup and progress of the investigation, and then detail the extension that this thesis will provide. Therefore, we will first describe the setup as done in the the paper, which has so far determined the thermodynamics involved, and derived the scalar perturbations of the system. What we hope to do now is to find the quasinormal modes associated with these perturbations and use them to determine the shape of the quantum critical region

4.1 Introduction

The basic setup is as follows; on the field theory side is a $2+1$ dimensional gauge theory related to the ABJM model [15], at finite chemical potential χ and mangnetic field B, and deformed by a triple trace operator Φ^3. The dual gravity theory is based on 4-dimensional $\mathcal{N}=2$ Fayet-Iliopoulos gauged supergravity, and the solutions considered are extremal, dyonic, asymptotically AdS_4 black branes, as well as a dyonic thermal gas solution.

The triple trace operator Φ^3, is dual to a a scalar field $\phi(r)$ in the bulk, where r is the holographic coordinate. r can be determined from an integration constant b, which is the vacuum expectation value (VeV) of Φ. The three main parameters of the solutions will therefore be b, χ, and B, and so we will try to define all equations in terms of these parameters.

4.2 Gravity setup

The gravity theory we will consider is the Einstein-Maxwell-scalar theory, consisting of two gauge fields and one real scalar field,

$$S=\frac{1}{\kappa^2}\int\sqrt{-g}d^4x\left(\frac{R}{2}-\frac{1}{2}\partial_\mu\phi\partial^\mu\phi-e^{\sqrt{6}\phi}\xi^3F^0_{\mu\nu}F^{0\mu\nu}-\frac{3}{\xi}e^{-\sqrt{\frac{2}{3}}\phi}F^1_{\mu\nu}F^{1\mu\nu}-V_g(\phi)\right)+S_{\text{GH}}, \tag{4.1}$$

where $\kappa^2=8\pi G_N$, S_{GH} is the Gibbons-Hawking term, g is the coupling constant, and ξ is determined by two constants $\xi=\sqrt{\frac{3\xi_0}{\xi_1}}$.

The scalar potential is,

$$V_g(\phi)=-\frac{3}{l^2_{AdS}}\cosh\left(\sqrt{\frac{2}{3}}\phi(r)\right), \tag{4.2}$$

where l_{AdS} is the AdS length scale given by $l^2_{AdS}=\frac{3\sqrt{3}}{2g^2\xi_0\xi_1^3}$.

From now on, we can set $\xi_0=\frac{1}{\sqrt{2}}$,$\xi_1=\frac{3}{\sqrt{2}}$, and $g=1$.

The **black brane** solution to 4.1 is,

$$ds^2 = -\frac{f(r)}{\sqrt{H_0(r)H_1(r)^3}}dt^2 + \sqrt{H_0(r)H_1(r)^3}\left(\frac{dr^2}{f(r)} + r^2(dx^2+dy^2)\right), \tag{4.3}$$

where x and y are two spatial directions. The metric functions are defined as,

$$H_0(r) = 1 - \frac{3b}{r}, \quad H_1(r) = 1 + \frac{b}{r}, \quad f(r) = \frac{c_1}{r} + \frac{c_2}{r^2} + r^2 H_0(r)H_1(r)^3, \tag{4.4}$$

and their coefficents are given by,

$$c_1 = \frac{Q^2 - B^2}{2b}, \quad c_2 = \frac{Q^2 + 3B^2}{2}. \tag{4.5}$$

Analysing the asymptotics of this metric we see that the conformal boundary is located at $r \to \infty$. The scalar field profile is found by solving Einstein's equations,

$$e^{\sqrt{\frac{8}{3}}\phi} = \frac{r+b}{r-3b}, \tag{4.6}$$

and the boundary behaviour of the scalar field is found to be,

$$\phi = \frac{\phi_-}{r} + \frac{\phi_+}{r^2} + O\left(\frac{1}{r^3}\right) \quad \text{as} \quad r \to \infty. \tag{4.7}$$

The dual field theory operator is the triple trace operator $\lambda\Phi^3$, and from the correspondence we know that ϕ_- is the expectation value of this operator, and ϕ_+ is related to the source of the operator. As shown in [16], the deformation by the triple trace operator corresponds to mixed boundary conditions,

$$\phi_+ = \lambda\phi_-^2. \tag{4.8}$$

Finally, the expression used for the chemical potential is,

$$\chi = -\int_{r_h}^{\infty} \tilde{F}^0_{tr} dr = -\frac{Q}{2(r_h - 3b)}. \tag{4.9}$$

As stated, one can also consider **thermal gas** type solutions to 4.1, which are found from the black brane solution by sending the horizon location to the singularity, which is $r_s = 3b$ for $b > 0$, and $r_s = -b$ for $b < 0$. Expanding around a black brane solution with $r_h = 3b + \epsilon$ $(b > 0)$ and $r_h = -b + \epsilon$ $(b > 0)$, and enforcing the condition $f(r_h) = 0$, the following quantities for the thermal gas solution can be obtained as $\epsilon \to 0$,

$$\begin{aligned} b_{TG} &= 2^{-\frac{7}{4}}\sqrt{|B|}, \quad Q_{TG} = 0, \quad \text{for} \quad b > 0 \\ b_{TG} &\propto \frac{B}{8\chi}, \quad Q_{TG} = 0, \quad \text{for} \quad b < 0 \end{aligned} \tag{4.10}$$

We have one issure with the $b < 0$ case that should be noted; when deriving the dependence of b_{TG} on B we had to make the identification between B and Q that is provided by the electromagnetic duality transformation. We do not yet know however, what the exact proportionality between the two is, so we cannot say for sure the precise relationship between b_{TG} and B. This is something we will resolve in the near future however.

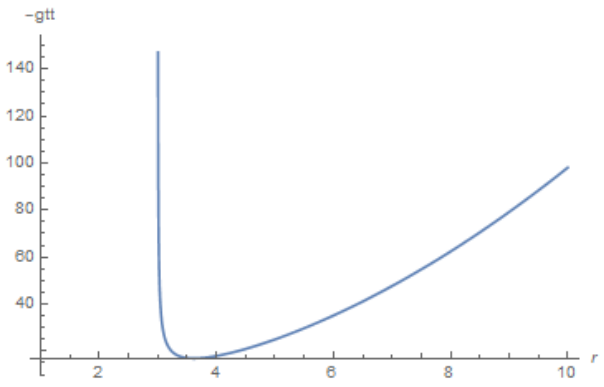

FIGURE 4.1: Black brane $-g_{tt}$ behaviour, with $b = 1, Q = 5, B = 1$. Here it can be seen that there is a divergence in the temporal component of the metric at $r = 3$

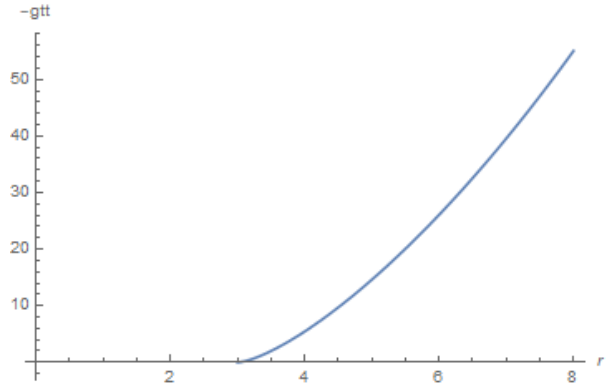

FIGURE 4.2: Thermal gas $-g_{tt}$ behaviour, with $b = 1$. It can be noticed how the horizon location is at $r = 3$, corresponding with the singularity location.

Finally the thermal gas solution itself is found to be,

$$ds^2_{\text{TG}} = -e^{\sqrt{6}\phi}\left(r^2 + 6br + 21b^2\right)dt^2 + e^{\sqrt{6}\phi}dr^2\left(r^2 + 6br + 21b^2\right)^{-1} + e^{\sqrt{6}\phi}(r-3b)^2(dx^2+dy^2),$$
$$e^{\sqrt{6}\phi} = \left(\frac{r+b}{r-3b}\right)^{\frac{3}{2}} \tag{4.11}$$

Figures 4.1 and 4.2 demonstrate the $-g_{tt}$ behaviour of the two solutions. It can be seen that the thermal gas solution is 'horizonless' as its horizon corresponds with the location of the singularity, and the black brane solution can be seen to diverge at this point, in these plots given by $r_{\text{h}} = 3$

4.3 $T \to 0$ thermodynamics

As shown in the paper, the free energy of the **black brane** can be found by noting that the free energy of any black brane is given by

$$F_{\text{BB}} = M_{\text{BB}} - TS_{\text{BB}} + Q_{\text{BB}}\chi, \tag{4.12}$$

where $M_{\text{BB}}, T, S_{\text{BB}}$ and Q_{BB} are the mass, temperature, entropy and charged of the black respectively. Using the horizon equation $f(r_{\text{h}}) = 0$ and the extremality equation $f'(r_{\text{h}}) = 0$, the free energy can be found in terms of our physical parameters (T, B, χ),

$$F_{\text{BB}} = \frac{27B^2 + 32\chi^4}{24\sqrt{6}|\chi|} \tag{4.13}$$

For the **thermal gas**, at vanishing temperature the entropy is also vanishing, and the free energy is found to be,

$$F_{\text{TG}} = M_{\text{TG}} = 2^{-\frac{1}{4}}|B|^{\frac{3}{2}}. \tag{4.14}$$

It is shown that these results respect the first law of thermodynamics.

In order to find the phase transition, we must look at where the free energies of the two solutions are the same. The difference in free energy is given by,

$$\Delta F = F_{\text{BB}} - F_{\text{TG}} = \frac{27B^2 + 32\chi^4}{24\sqrt{6}|\chi|} - 2^{-\frac{1}{4}}|B|^{\frac{3}{2}}, \tag{4.15}$$

and it vanishes at,

$$|B_c| = \frac{4\sqrt{2}\chi^2}{3}. \tag{4.16}$$

The non-analyticity arises in the second derivatives and hence the phase transition is of second order. With this, we have proof of the existence of a second order quantum phase transition, as all of this analysis was done with $T = 0$.

The next step of the thesis is now to analyse the phase transition using the quasinormal modes, however it should be noted that this thermodynamic analyses was carried out for $b > 0$, so for $b < 0$ the QCP could be located at a different B_c

4.4 Quasinormal modes

4.4.1 Fluctuations

Based on the analysis in chapter three, we know that the black brane is going to be dual to a field theory at finite temperature, and the quasinormal modes of this black brane can be used to uncover interesting information about the dual field theory. In order to calculate the quasinormal modes of the black brane, we need to derive the fluctuation equations for the type of perturbations being considered. We will first consider the simplest case of a massless scalar perturbation to the background 4.3. The scalar fluctuation equation can be found from the massless scalar action as in 3.20,

$$\partial_\mu \left(g^{\mu\nu} \sqrt{-g} \partial_\nu \delta\phi \right) = 0. \tag{4.17}$$

As stated earlier, in order to use the mathematica code from [13], we must change coordinates to Eddington Finklestein coordinates and redefine the radial coordinate such that the horizon is located at $r_{\text{new}} = 1$ and the boundary is located at $r_{\text{new}} = 0$. So we begin by changing to Eddington Finklestein coordinates, in which the background 4.3 becomes,

$$ds^2 = -\frac{f(r)}{\sqrt{H_0(r)H_1(r)^3}} dt^2 - 2drdt + r^2(dx^2 + dy^2). \tag{4.18}$$

Next we define the coordinate,

$$r = \frac{1}{uu_h}, \tag{4.19}$$

where u_h is the location of the horizon in these coordinates. Expressed this way, we see that the horizon and boundary conditions are now defined by $u = 1$ and $u = 0$ respectively. In these coordinates, the metric now reads,

$$ds^2 = -\frac{f(u)}{\sqrt{H_0(u)H_1(u)^3}} dt^2 + \frac{2}{u^2 u_h} dudt + \frac{1}{(uu_h)^2}(dx^2 + dy^2), \tag{4.20}$$

with the metric functions now becoming,

$$H_0(u) = 1 - 3buu_h, \quad H_1(u) = 1 + buu_h, \quad f(u) = c_1 uu_h + c_2(uu_h)^2 + \frac{1}{(uu_h)^2} H_0(u)H_1(u)^3, \tag{4.21}$$

We choose these coordinates for two reasons, the first is that the Eddington-Finklestein coordinates ensure that the horizon boundary conditions are satisfies, they only demand that the solutions be regular at the horizon. The second reason is simply a numerical one, we change the radial coordinate as above so that our boundary now lies at a finite interval, which makes the numerics simpler. With all of this

taken into account, the equation of motion 4.17 is now,

$$\begin{aligned}
&\Big[2+8b^3u_h^3-c_1u_h^3+26b^4u_h^4-2c_2u_h^4+12b^5u_h^5-3b^2u_h^2(4+c_1u_h^3\\
&+2bu_h(-2+c_1u_h^3+2c_2u_h^4))(q^2u\sqrt{1-3buu_h}(2+8b^3u_h^3-c_1uh^3\\
&+26b^4u_h^4-2c_2u_h^4+12b^5u_h^5-3b^2u_h^2(4+c_1u_h^3)+2bu_h(-2+c_1u_h^3\\
&+2c_2u_h^4))-4i(1-3bu_h)^{3/2}(1+bu_h)^{5/2}\sqrt{1+buu_h}(-1+2buu_h)\lambda)\cdot\\
&\Big(\frac{1}{4u^3u_h^3(1+bu_h)^5(-1+3bu_h)^3\sqrt{1-3buu_h}}\Big)\Big]\boldsymbol{\delta\phi(u)}\\
&+\Big[\Big(-3buu_h(1+buu_h)^3+\frac{3bu^4u_h^4(c_1+c_2uu_h)}{-1+3buu_h}+\frac{3buu_h((1-3buu_h)(1+buu_h)^3+u^3u_h^3(c_1+c_2uu_h)\ )}{1+buu_h}\\
&+\Big(4+16b^3u^3u_h^3-2c_1u^3u_h^3+52b^4u^4u_h^4-4c_2u^4u_h^4+24b^5u^5u_h^5-6b^2u^2u_h^2\ (4+c_1u^3u_h^3)+\\
&+4buu_h\left(-2+c_1u^3u_h^3+2c_2u^4u_h^4\right)\Big)\cdot\\
&\Big(\frac{1}{(1+buu_h)(-1+3buu_h)}\Big)\\
&+\Big(2iu\sqrt{1-3buu_h}(1+buu_h)^{3/2}(2+8b^3u_h^3-c_1u_h^3+26b^4u_h^4-2c_2u_h^4\\
&+12b^5u_h^5-3b^2u_h^2(4+c_1u_h^3)+2bu_h(-2+c_1u_h^3+2c_2u_h^4)\ )\lambda\Big)\frac{1}{(1-3bu_h)^{3/2}(1+bu_h)^{5/2}2u^3u_h^3}\Big]\boldsymbol{\delta\phi'(u)}\\
&+\left(-8b^3u+c_1u+\frac{1}{u^2u_h^3}-\frac{6b^2}{u_h}-3b^4u^2u_h+c_2u^2u_h\right)\boldsymbol{\delta\phi''(u)}\\
&=0
\end{aligned}\tag{4.22}$$

where we have again taken the plane wave solution for the fluctuation, $\delta\phi = e^{-i(kx-\omega t)}\delta\phi(u)$, and there has been a rescaling $\omega = 2\pi T\lambda$ and $k = 2\pi Tq$. T is the temperature of the black brane, and it is found from $T = -u_h\frac{h'(1)}{4\pi}$, where $h(r)$ is the blackening factor of the black brane.

With the bare fluctuation equation at hand, the next step is to determine the boundary behaviour of the scalar field, and rescale it appropriately such that it approaches zero linearly towards the boundary. This can be achieved by taking the ansatz $\delta\phi(u) \propto u^p$, inserting it into equation 4.22, and solving for p as $u \to 0$. There are two solutions, $p \to 0$ and $p \to 3$, which leads to two solutions for the scalar field at the boundary,

$$\delta\phi_1(u) = 1, \quad \delta\phi_2(u) = u^3. \tag{4.23}$$

$\delta\phi_1$ is clearly the non-normalizable solution that was discussed earlier, so we discard this one using the Dirichler boundary conditions, and keep $\delta\phi_2$. In order for the scalar to approach zero linearly at the boundary, it must be rescaled as,

$$\delta\tilde{\phi} = u^2\delta\phi, \tag{4.24}$$

and finally the equation itself should be rescaled by a factor of u^2 so that it becomes a constant on the boundary. With all of this taken into account, the final fluctuation equation is,

$$\begin{aligned}
&\Bigg[2u^2\ \left(-8b^3u+c_1u+\frac{1}{u^2u_h^3}-\frac{6b^2}{u_h}-3b^4u^2u_h+c_2u^2u_h\right)\\
&+u\left(2+8b^3u_h^3-c_1u_h^3+26b^4u_h^4-2c_2u_h^4+12b^5u_h^5-3b^2u_h^2\left(4+c_1u_h^3\right)+\right.\\
&2bu_h\left(-2+c_1u_h^3+2c_2u_h^4\right)\left(q^2u\sqrt{1-3buu_h}\left(2+8b^3u_h^3-c_1u_h^3+26b^4u_h^4-\right.\right.\\
&\left.\left.2c_2u_h^4+12b^5u_h^5-3b^2u_h^2\left(4+c_1u_h^3\right)+2bu_h\left(-2+c_1u_h^3+2c_2u_h^4\right)-\right.\right.\\
&\left.\left.4i(1-3bu_h)^{3/2}(1+bu_h)^{5/2}\sqrt{1+buu_h}(-1+2buu_h)\lambda\right)\cdot\right.\\
&\left.\frac{1}{4u_h^3(1+bu_h)^5(-1+3bu_h)^3\sqrt{1-3buu_h}}\right.\\
&+\frac{1}{u^3}\left(-3buu_h(1+buu_h)^3+\frac{3bu^4u_h^4(c_1+c_2uu_h)}{-1+3buu_h}+\frac{3buu_h\left((1-3buu_h)(1+buu_h)^3+u^3u_h^3(c_1+c_2uu_h)\right)}{1+buu_h}\right.\\
&+\left(4+16b^3u^3u_h^3-2c_1u^3u_h^3+52b^4u^4u_h^4-4c_2u^4u_h^4+24b^5u^5u_h^5-6b^2u^2u_hu_h^2\left(4+c_1u^3u_h^3\right)\right.\\
&\left.\left.+4buu_h\left(-2+c_1u^3u_h^3+2c_2u^4u_h^4\right)\right)\cdot\frac{1}{(1+buu_h)(-1+3buu_h)}\right.\\
&\left.+\frac{2iu\sqrt{1-3buu_h}(1+buu_h)^{3/2}}{(1-3bu_h)^{3/2}(1+bu_h)^{5/2}}\cdot\right.\\
&\left.\left(2+8b^3u_h^3-c_1u_h^3+26b^4u_h^4-2c_2u_h^4+12b^5u_h^5-3b^2u_h^2\left(4+c_1u_h^3\right)+2bu_h\left(-2+c_1u_h^3+2c_2u_h^4\right)\right)\lambda\right)\Bigg]\delta\tilde{\boldsymbol{\phi}}(\boldsymbol{u})\\
&+\Bigg[4u^3(-8b^3u+c_1u+\frac{1}{u^2u_h^3}-\frac{6b^2}{u_h}-3b^4u^2u_h+c_2u^2u_h)\\
&+\frac{u}{2u_h^3}(-3buuh(1+buu_h)^3+\frac{3bu^4uh^4(c_1+{}_2uu_h)}{-1+3buu_h}\\
&+\frac{3buu_h((1-3buu_h)(1+buu_h)^3+u^3u_h^3(c_1+c_2uu_h))}{1+buu_h}\\
&(4+16b^3u^3u_h^3-2c_1u^3u_h^3+52b^4u^4u_h^4-4c_2u^4u_h^4+24b^5u^5u_h^5-6b^2u^2u_h^2\left(4+c_1u^3u_h^3\right)+4buuh\left(-2+c_1u^3u_h^3\right.\\
&\left.+2c_2u^4u_h^4\right))\cdot\frac{1}{(1+buu_h)(-1+3buu_h)}\\
&+\left(\frac{2iu\sqrt{1-3buu_h}(1+buu_h)^{3/2}}{(1-3bu_h)^{3/2}(1+bu_h)^{5/2}}\right)\left(2+8b^3u_h^3-c_1u_h^3+26b^4u_h^4\right.\\
&\left.-2c_2u_h^4+12b^5u_h^5-3b^2u_h^2\left(4+c_1u_h^3\right)+2bu_h\left(-2+c_1u_h^3+2c_2u_h^4\right)\right)\lambda\Bigg]\delta\tilde{\boldsymbol{\phi}}'(\boldsymbol{u})\\
&+u^4\left(-8b^3u+c_1u+\frac{1}{u^2u_h^3}-\frac{6b^2}{u_h}-3b^4u^2u_h+c_2u^2u_h\right)\delta\tilde{\boldsymbol{\phi}}''(\boldsymbol{u})
\end{aligned}\tag{4.25}$$

To run the code that calculates the quasinormal modes, we must now specify the parameter values. As stated earlier, we want the final equations to depend on the physical parameters (B, b, χ), so we want to express the final equations as a function of these parameters, which can then be specified. To do all

of this, we make use of the following equations,

$$\chi = -\frac{Q}{2(u_{\rm h}^{-1} - 3b)}, \tag{4.26}$$

$$f(1) = 0 \quad \text{(horizon condition)} \tag{4.27}$$

Using equation 4.26, it is possible to rewrite the fluctuation equation as a function of B, b, χ and $u_{\rm h}$. Next, $u_{\rm h}$ needs to be determined by solving equation 4.27,

$$\frac{\sqrt{1-3bu_{\rm h}}(1+bu_{\rm h})^{3/2}}{u_{\rm h}^2} + \frac{\frac{\left(-B^2+4\left(-3b+\frac{1}{u_{\rm h}}\right)^2\right)u_{\rm h}}{2b} + \frac{1}{2}\left(3B^2+4\left(-3b+\frac{1}{u_{\rm h}}\right)^2\right)u_{\rm h}^2}{\sqrt{1-3bu_{\rm h}}(1+bu_{\rm h})^{3/2}} = 0, \tag{4.28}$$

but this equation has three roots, and the correct one must be selected, correct meaning it must be positive and real. Furthermore, if there are multiple solutions meeting these criteria then the minimum of these is the valid solution, as this corresponds to the maximum $r_{\rm h}$ in the r coordinate. Finally, there is one more condition that must be imposed, as the value of $u_{\rm h}$ depends on the sign of b. In order to avoid singularities in the metric, we require that the functions H_0 and H_1 be non-zero, and from 4.21 this implies that,

$$\begin{aligned} u_{\rm h} &< \frac{1}{3b} \quad \text{if} \quad b > 0, \\ u_{\rm h} &< -\frac{1}{b} \quad \text{if} \quad b < 0. \end{aligned} \tag{4.29}$$

This is implemented in the code, and the correct horizon location is obtained and then used in the fluctuation equation, which is now a function of B, b and χ. Now we are ready to calculate the quasinormal modes; as a first demonstration, the values $b = .1, B = 3, k \to 0$ were taken, and the following modes were found using the *GetModes* function described in section 3.3,

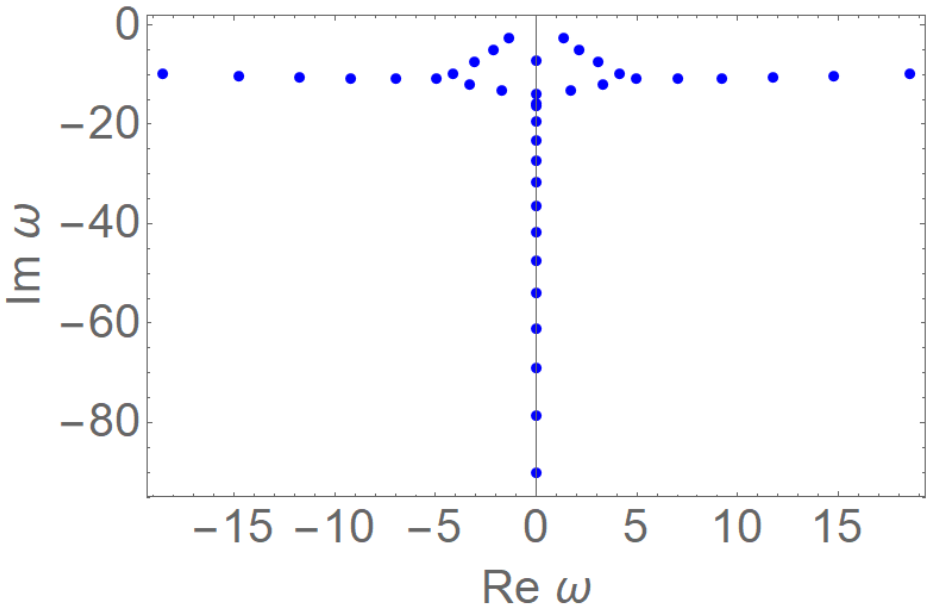

FIGURE 4.3: Massless scalar quasinormal mode spectrum with $b = .1$ and $B = 3$ using GetModes.

As discussed before, this function does not produce the most accurate results for the modes, some

of them being numerical artifacts, so we next find a more accurate solution using the function *GetAccurateModes*, which results in the spectrum shown in figure 4.4.

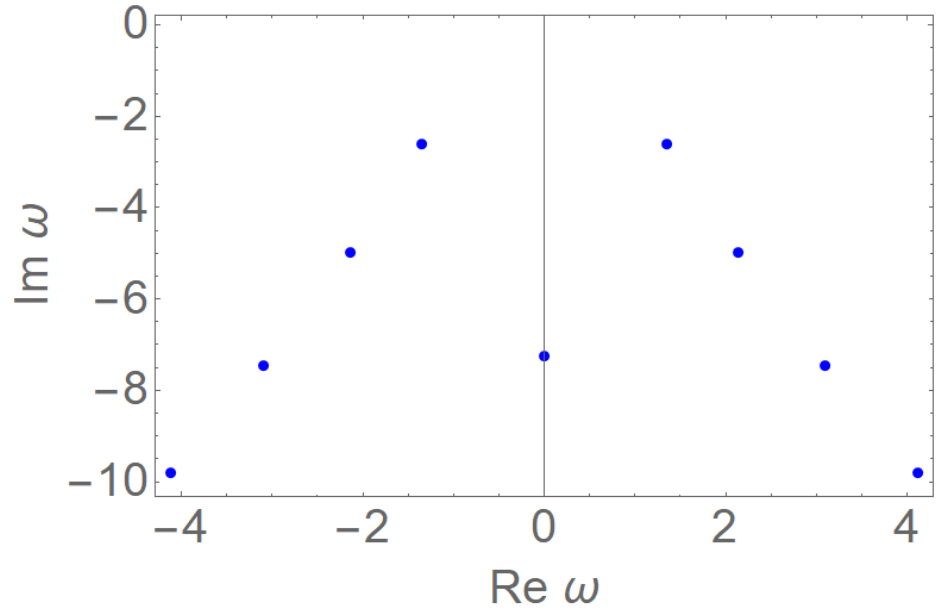

FIGURE 4.4: Massless scalar quasinormal mode spectrum with $b = .1$ and $B = 3$, using GetAccurateModes. This clearly gives a more accurate solution for the modes, and their symmetric nature can be observed.

Finally, just to check that everything is correct, we can check that the eigenfunctions are in fact smooth and obey the conditions we imposed. Figure 4.5 shows the behaviour of the eigenfunctions, which we can see are smooth and go to 1 on the horizon and 0 on the boundary, as expected from the rescalings carried out.

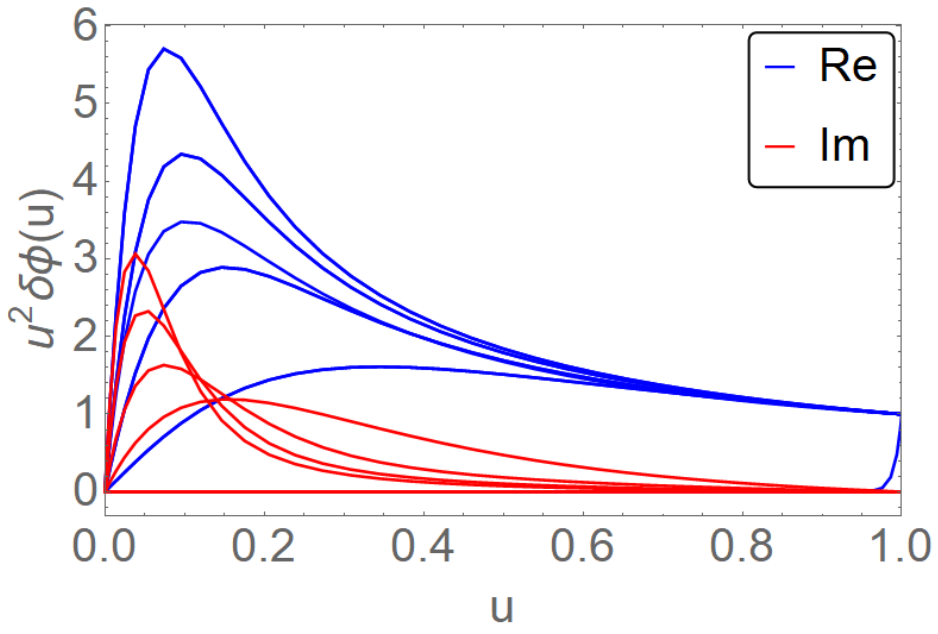

FIGURE 4.5: Eigenfunctions associated with the above quasinormal modes. They are well behaved and have the correct boundary behaviour. Only the positive imaginary part of the modes are shown for convenience.

4.5 Quantum critical region

The next goal of the thesis is to use these quasinormal modes to determine the quantum critical region associated with the quantum phase transition. This essentially requires us to find the temperature as a function of the magnetic field, which we can do with the following equations,

$$\chi = -\frac{Q}{2(r_h - 3b)}, \tag{4.30}$$

$$f(r_h) = 0 \quad \text{(horizon condition)}, \tag{4.31}$$

$$T = \frac{f'(r_h)}{4\pi} \quad \text{(Hawking temperature)}, \tag{4.32}$$

$$\omega_I = \Delta b, \quad \text{where} \quad \Delta b = b_{TG} - b_{BB} \tag{4.33}$$

where b_{BB} is b for the black brane, which is unknown, and b_{TG} is b for the thermal gas as given in equation 4.10. With these three equations at hand we can begin to get everything as a function of the relevant parameters. First we will try to get a simple analytic expression of the temperature in terms of r_h, B, χ and b, where r_h and b will be later eliminated by other equations. It is useful to make the following rescalings to simplify the equations,

$$\bar{r}_h = \frac{r_h}{b}, \quad \bar{Q} = \frac{Q}{b^2} \quad \bar{B} = \frac{B}{b^2}, \quad \bar{T} = \frac{T}{b}, \quad \bar{\chi} = \frac{\chi}{b}. \tag{4.34}$$

Using equation 4.31 in our rescaled coordinates, we can find the following equation,

$$\bar{Q}^2(\bar{r}_h + 1) - \bar{B}^2(\bar{r}_h - 3) + 2(\bar{r}_h - 3)(1 + \bar{r}_h)^3 = 0. \tag{4.35}$$

Next, with equation 4.32 an expression for the temperature can be found,

$$\bar{T} = \frac{(\bar{r}_h - 3)\left(\bar{B}^2(\bar{r}_h - 5) + 4(\bar{r}_h - 2)(1 + \bar{r}_h)^3\right) - (\bar{r}_h^2 - 1)\bar{Q}^2}{8\pi(1 + \bar{r}_h)^{\frac{5}{2}}(\bar{r}_h - 3)^{\frac{3}{2}}}, \tag{4.36}$$

and rewriting the $(\bar{r}_h^2 - 1)$ term at the end, we can use the previous equation we found and substitute,

$$\bar{Q}^2(\bar{r}_h + 1) = -\bar{B}^2(\bar{r}_h - 3) - 2(\bar{r}_h - 3)(1 + \bar{r}_h)^3 \tag{4.37}$$

into the temperature to get,

$$\bar{T} = \frac{(\bar{r}_h - 3)\left(\bar{B}^2(\bar{r}_h - 5) + 4(\bar{r}_h - 2)(1 + \bar{r}_h)^3\right) + \left(\bar{B}^2(3 - \bar{r}_h) + 2(\bar{r}_h - 3)(1 + \bar{r}_h)^3\right)(\bar{r}_h - 1)}{8\pi(1 + \bar{r}_h)^{\frac{5}{2}}(\bar{r}_h - 3)^{\frac{3}{2}}}. \tag{4.38}$$

This can be further simplified to give us the following expression for the temperature,

$$\bar{T} = \frac{-2\bar{B}^2 + (1 + \bar{r}_h)^3(3\bar{r}_h - 5)}{4\pi(1 + \bar{r}_h)^{\frac{5}{2}}(\bar{r}_h - 3)^{\frac{1}{2}}}, \tag{4.39}$$

and we will just reintroduce b later when we have found all the other relevant formulations of the parameters.

4.5.1 Horizons

We now must determine the horizon distance r_h in terms of B, b and χ. Taking equation 4.37, reintroducing b, and subbing in equation 4.30 we find,

$$B^2 - 2b(b + r_h)^3 + 4(3b - r_h)(b + r_h)\chi^2 = 0. \tag{4.40}$$

Solving this equation for r_h, we find there are three roots, the largest of which being the desired solution. There are **two classes of solutions**; those where $b > 0$ and those with $b < 0$, and we need to analyse the root behaviour in both cases before we make use of them.

$b < 0$ case

We first consider $b < 0$, figure 4.6 shows a plot of the roots over a range of b and B values.

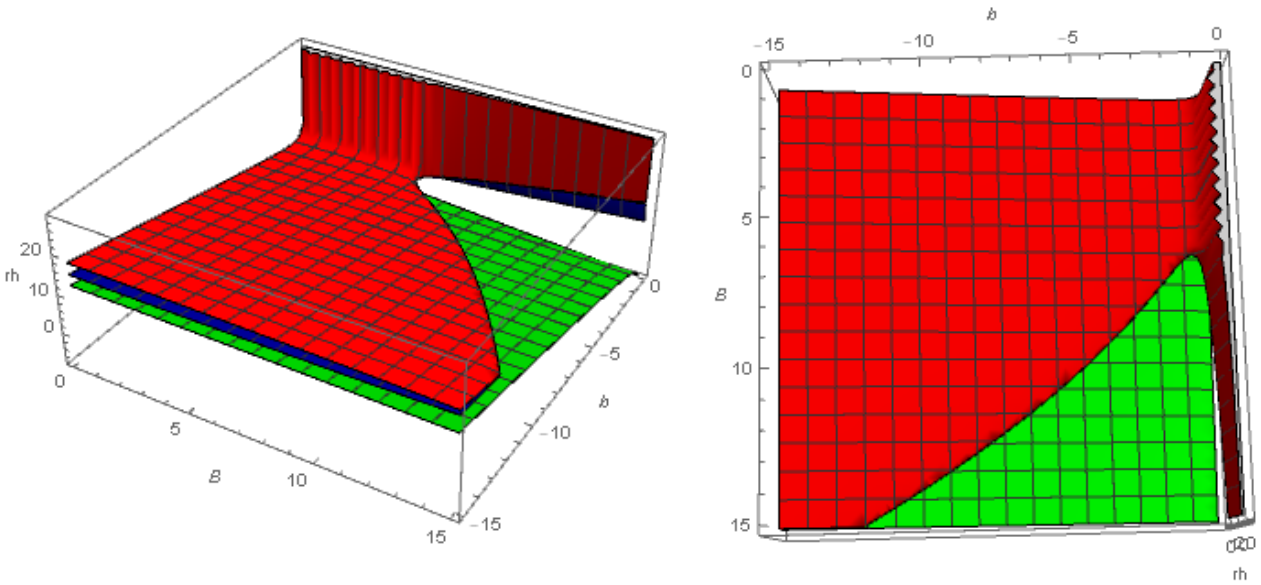

FIGURE 4.6: Here we see the three horizon solutions for negative values of b. The first root is the red surface, the second the green surface, and the third the blue surface. It can be seen that the first root is always the largest, except in a certain region as shown in the second figure, where in fact there is no valid root as the next largest root is negative in this region.

We can clearly see that the first solution is always the largest one, and this continues for larger ranges of values, however there is always a range of values of B and b for which there is no positive solution, and so there is no horizon. This region grows as we increase the range of values, and so imposes a restriction on what values of b and B we consider. In this particular range of values, we see that for approximately $5.5 < B < 15$ and $-12 < b < -1$, there is no horizon, and so we must take this into account when performing later calculations.

With this in mind we consider the first root, given by

$$r_{\rm h} = -\frac{3b^2+2\chi^2}{3b} + \\ + \frac{-96b^2\chi^2-16\chi^4}{3\,2^{2/3}b\sqrt[3]{-108b^2B^2+1152b^2\chi^4+128\chi^6+\sqrt{4\left(-96b^2\chi^2-16\chi^4\right)^3+\left(-108b^2B^2+1152b^2\chi^4+128\chi^6\right)^2}}} - \\ - \frac{\sqrt[3]{-108b^2B^2+1152b^2\chi^4+128\chi^6+\sqrt{4\left(-96b^2\chi^2-16\chi^4\right)^3+\left(-108b^2B^2+1152b^2\chi^4+128\chi^6\right)^2}}}{6\sqrt[3]{2}b}. \tag{4.41}$$

In order for this root to remain real, the terms under the square root need to amount to a positive number. Looking at the square root inside this square root, we can find out the maximum value that B can take by finding the roots of

$$4\left(-96b^2\chi^2-16\chi^4\right)^3+\left(-108b^2B^2+1152b^2\chi^4+128\chi^6\right)^2=0, \tag{4.42}$$

which are found to be

$$\begin{aligned} B &\to \frac{-4}{3}\sqrt{\frac{2}{3}}\sqrt{9\chi^4+\frac{\chi^6}{b^2}-\frac{\sqrt{\chi^6\left(6b^2+\chi^2\right)^3}}{b^2}}, \\ B &\to \frac{4}{3}\sqrt{\frac{2}{3}}\sqrt{9\chi^4+\frac{\chi^6}{b^2}-\frac{\sqrt{\chi^6\left(6b^2+\chi^2\right)^3}}{b^2}}, \\ B &\to \frac{-4}{3}\sqrt{\frac{2}{3}}\sqrt{9\chi^4+\frac{\chi^6}{b^2}+\frac{\sqrt{\chi^6\left(6b^2+\chi^2\right)^3}}{b^2}}, \\ B &\to \frac{4}{3}\sqrt{\frac{2}{3}}\sqrt{9\chi^4+\frac{\chi^6}{b^2}+\frac{\sqrt{\chi^6\left(6b^2+\chi^2\right)^3}}{b^2}}, \end{aligned} \tag{4.43}$$

of which we take the last root, as it is the only one to give a positive real solution. So we now have a formula to determine the maximum value of B we can have for a given value of b and χ, which is useful as it will help us avoid the horizonless region from before when we are performing later calculations.

$$B_{\rm max} = \frac{4}{3}\sqrt{\frac{2}{3}}\sqrt{9\chi^4+\frac{\chi^6}{b^2}+\frac{\sqrt{\chi^6\left(6b^2+\chi^2\right)^3}}{b^2}} \tag{4.44}$$

Figure 4.7 below shows the behaviour of the B limit as b changes, this behaviour will be an important consideration later when computing the quasinormal modes.

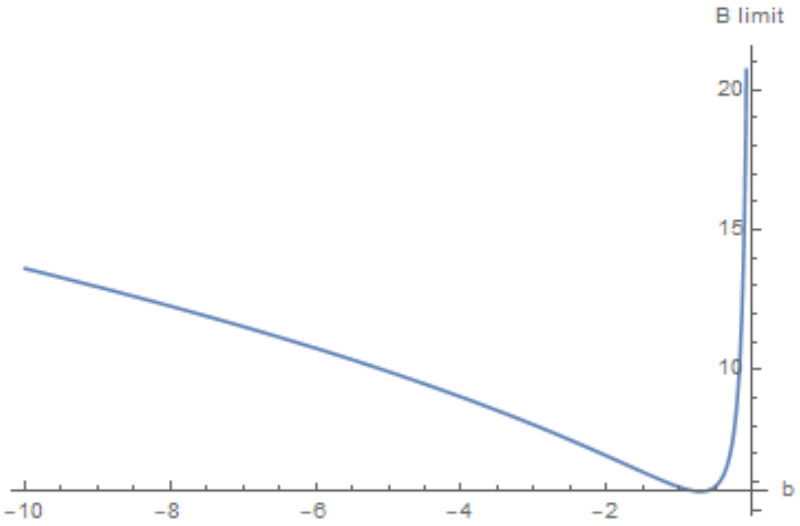

FIGURE 4.7: The maximum value B can be for $b < 0$

As a quick demonstration, if we set $b = -5$ and $\chi = 1$, we find that $B_{\max} = 9.93375$, and if we look again at figure 4.6 we see that this is exactly the boundary of the horizonless region.

With this analysis at hand we are prepared to perform any calculations involving $b < 0$, we can now plug this first solution for r_h into our expression for T to get,

$$T = \left[-\frac{4B^2}{b^3} - 2b\left(-8 - \frac{2\chi^2}{b^2} - \frac{8\sqrt[3]{2}(6b^2\chi^2+\chi^4)}{b^2\sqrt[3]{-108b^2B^2+1152b^2\chi^4+128\chi^6+4\sqrt{-1024(6b^2\chi^2+\chi^4)^3+(32\chi^6-9b^2(3B^2-32\chi^4))^2}}} - \frac{\sqrt[3]{-108b^2B^2+1152b^2\chi^4+128\chi^6+\sqrt{4(-96b^2\chi^2-16\chi^4)^3+(-108b^2B^2+1152b^2\chi^4+128\chi^6)^2}}}{2\sqrt[3]{2}b^2}\right)\cdot \left(\frac{2\chi^2}{3b^2} + \frac{4\,2^{2/3}(6b^2\chi^2+\chi^4)}{3b^2\sqrt[3]{32\chi^6-9b^2(3B^2-32\chi^4)+3\sqrt{3}\sqrt{-b^2(8192b^4\chi^6+64B^2\chi^6+b^2(-27B^4+576B^2\chi^4+1024\chi^8))}}} + \frac{\sqrt[3]{-108b^2B^2+1152b^2\chi^4+128\chi^6+4\sqrt{-1024(6b^2\chi^2+\chi^4)^3+(32\chi^6-9b^2(3B^2-32\chi^4))^2}}}{6\sqrt[3]{2}b^2}\right)^3\right]$$

$$\left[8\pi\sqrt{-4-\frac{2\chi^2}{3b^2} - \frac{42^{2/3}(6b^2\chi^2+\chi^4)}{3b^2\sqrt[3]{32\chi^6-9b^2(3B^2-32\chi^4)+3\sqrt{3}\sqrt{-b^2(8192b^4\chi^6+64B^2\chi^6+b^2(-27B^4+576B^2\chi^4+1024\chi^8))}}} - \frac{\sqrt[3]{-108b^2B^2+1152b^2\chi^4+128\chi^6+4\sqrt{-1024(6b^2\chi^2+\chi^4)^3+(32\chi^6-9b^2(3B^2-32\chi^4))^2}}}{6\sqrt[3]{2}b^2}}\cdot \left(-\frac{2\chi^2}{3b^2} - \frac{42^{2/3}(6b^2\chi^2+\chi^4)}{3b^2\sqrt[3]{32\chi^6-9b^2(3B^2-32\chi^4)+3\sqrt{3}\sqrt{-b^2(8192b^4\chi^6+64B^2\chi^6+b^2(-27B^4+576B^2\chi^4+1024\chi^8))}} - \frac{\sqrt[3]{-108b^2B^2+1152b^2\chi^4+128\chi^6+4\sqrt{-1024(6b^2\chi^2+\chi^4)^3+(32\chi^6-9b^2(3B^2-32\chi^4))^2}}}{6\sqrt[3]{2}b^2}\right)^{5/2}\right]^{-1} \tag{4.45}$$

$b > 0$ case

Similarly, for $b > 0$ we we find three roots, except this time the second root is always the largest, as shown in figure 4.8. In this figure the colour scheme is the same as in the $b < 0$ case, and the additional sheer black surface that represents $r_h = 0$.

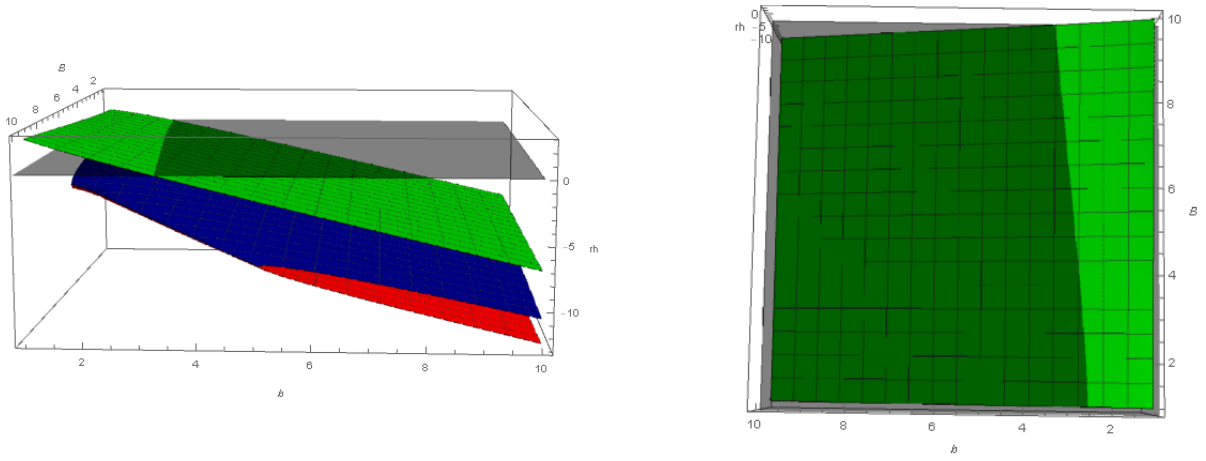

FIGURE 4.8: Here we see the three horizon solutions for positive values of b. The first root is the red surface, the second the green surface, and the third the blue surface. It can be seen that the second root is always the largest, however there is a very large range of values for which it is negative. The sheer black surface shows where $r_h = 0$.

Clearly there is quite a large range of values for which the solution is negative, so similar to earlier these combinations must be avoided. As done for the $b < 0$ case, we can derive a limit for the magnetic field, by imposing the realness and positivity of the horizon. We find that in this case these conditions impose a limit on how small B can be, namely

$$B_{\text{min}} = \frac{\sqrt{2}b\sqrt{b^2 - 6\chi^2}\left(6b^2 + \chi^2\right)^{3/2}}{\sqrt{216b^6 + 108b^4\chi^2 + 18b^2\chi^4 + \chi^6}}. \tag{4.46}$$

To demonstrate, take $\chi = 1$ and $b = 3$ and we find that $B_{\text{min}} = 7.34847$. Inspecting figure 4.8 above we see that this indeed defines the point at which we reach the boundary of the positive solution, where any lower value of B gives a negative solution. With these considerations in place we can now use the second solution to compute T, the equation for this horizon is given by,

$$r_h = -\frac{3b^2 + 2\chi^2}{3b} - \frac{\left(1 + i\sqrt{3}\right)\left(-96b^2\chi^2 - 16\chi^4\right)}{6\,2^{2/3}b\sqrt[3]{-108b^2B^2 + 1152b^2\chi^4 + 128\chi^6 + \sqrt{4\left(-96b^2\chi^2 - 16\chi^4\right)^3 + \left(-108b^2B^2 + 1152b^2\chi^4 + 128\chi^6\right)^2}}} + \frac{\left(1 - i\sqrt{3}\right)\sqrt[3]{-108b^2B^2 + 1152b^2\chi^4 + 128\chi^6 + \sqrt{4\left(-96b^2\chi^2 - 16\chi^4\right)^3 + \left(-108b^2B^2 + 1152b^2\chi^4 + 128\chi^6\right)^2}}}{12\sqrt[3]{2}b}, \tag{4.47}$$

and the temperature using this root is given by

$$
\begin{aligned}
T = \Bigg[b\Bigg(-\frac{4B^2}{b^4} + 2\Bigg(-\frac{2\chi^2}{3b^2} + \\
\frac{2\,2^{2/3}(1+i\sqrt{3})(6b^2\chi^2+\chi^4)}{3b^2\sqrt[3]{32\chi^6 - 9b^2(3B^2-32\chi^4) + 3\sqrt{3}\sqrt{-b^2(8192b^4\chi^6 + 64B^2\chi^6 + b^2(-27B^4+576B^2\chi^4+1024\chi^8))}}} \\
+ \frac{(1-i\sqrt{3})\sqrt[3]{-108b^2B^2 + 1152b^2\chi^4 + 128\chi^6 + 4\sqrt{-1024(6b^2\chi^2+\chi^4)^3 + (32\chi^6 - 9b^2(3B^2-32\chi^4))^2}}}{12\sqrt[3]{2}b^2}\Bigg)^3 . \\
\Bigg(-8 - \frac{2\chi^2}{b^2} + \frac{2\,2^{2/3}(1+i\sqrt{3})(6b^2\chi^2+\chi^4)}{b^2\sqrt[3]{32\chi^6 - 9b^2\,(3B^2-32\chi^4) + 3\sqrt{3}\sqrt{-b^2\,(8192b^4\chi^6 + 64B^2\chi^6 + b^2\,(-27B^4+576B^2\chi^4+1024\chi^8))}}} \\
+ \frac{(1-i\sqrt{3})\sqrt[3]{-108b^2B^2 + 1152b^2\chi^4 + 128\chi^6 + 4\sqrt{-1024(6b^2\chi^2+\chi^4)^3 + (32\chi^6 - 9b^2(3B^2-32\chi^4))^2}}}{4\sqrt[3]{2}b^2}\Bigg)\Bigg) \Bigg] \\
\Bigg[\Bigg(8\pi\sqrt{-4 - \frac{2\chi^2}{3b^2} + \frac{2\,2^{2/3}(1+i\sqrt{3})(6b^2\chi^2+\chi^4)}{3b^2\sqrt[3]{32\chi^6 - 9b^2(3B^2-32\chi^4) + 3\sqrt{3}\sqrt{-b^2(8192b^4\chi^6 + 64B^2\chi^6 + b^2(-27B^4+576B^2\chi^4+1024\chi^8))}}} \\
+ \frac{\left(1-i\sqrt{3}\right)\sqrt[3]{-108b^2B^2 + 1152b^2\chi^4 + 128\chi^6 + 4\sqrt{-1024\,(6b^2\chi^2+\chi^4)^3 + (32\chi^6 - 9b^2\,(3B^2-32\chi^4))^2}}}{12\sqrt[3]{2}b^2} \cdot \\
\Bigg(-\frac{2\chi^2}{3b^2} + \frac{22^{2/3}(1+i\sqrt{3})(6b^2\chi^2+\chi^4)}{3b^2\sqrt[3]{32\chi^6 - 9b^2(3B^2-32\chi^4) + 3\sqrt{3}\sqrt{-b^2(8192b^4\chi^6 + 64B^2\chi^6 + b^2(-27B^4+576B^2\chi^4+1024\chi^8))}}} \\
+ \frac{(1-i\sqrt{3})\sqrt[3]{-108b^2B^2 + 1152b^2\chi^4 + 128\chi^6 + 4\sqrt{-1024(6b^2\chi^2+\chi^4)^3 + (32\chi^6 - 9b^2(3B^2-32\chi^4))^2}}}{12\sqrt[3]{2}b^2}\Bigg)^{5/2}\Bigg]^{-1}
\end{aligned}
\tag{4.48}
$$

4.5.2 Temperature profile

It will also be useful to note the behaviour of the temperature over the same range of b and B values for the fixed $\chi = 1$ slice. For $\boldsymbol{b < 0}$, the temperature profile is as shown in figure 4.9. From this we can see a clear region where the temperature appears to be tending towards zero, and this region becomes larger as B and b are increased.

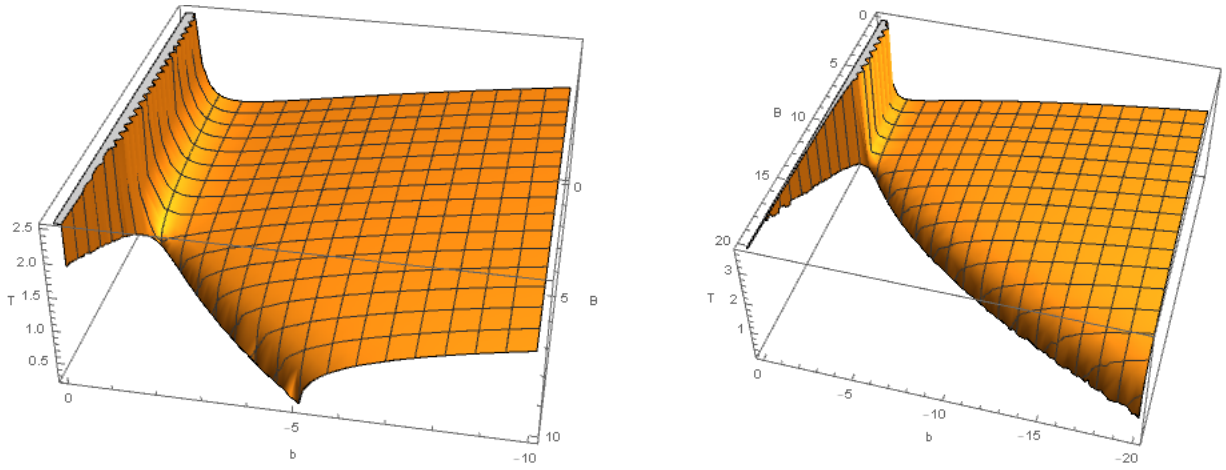

FIGURE 4.9: Temperature behaviour for $b < 0$. It can be seen how $T \to 0$ approximately along the same line that we determined gave the maximum value for B. On the left we can see how this line extends as B increases and b becomes more negative. The shape of the region is similar to that of the allowed horizon values, which makes sense as these are used in computing the temperature.

If we compare this to the limit found for the maximum value, we see that the curves seem to coincide. We see that the B limit seems to define the $T \sim 0$ line (numerically extracted), figure 4.10 below further support this. Seeing as this limit ultimately comes from the allowed horizon values, and that the temperature depends on this, the shape of the region makes sense.

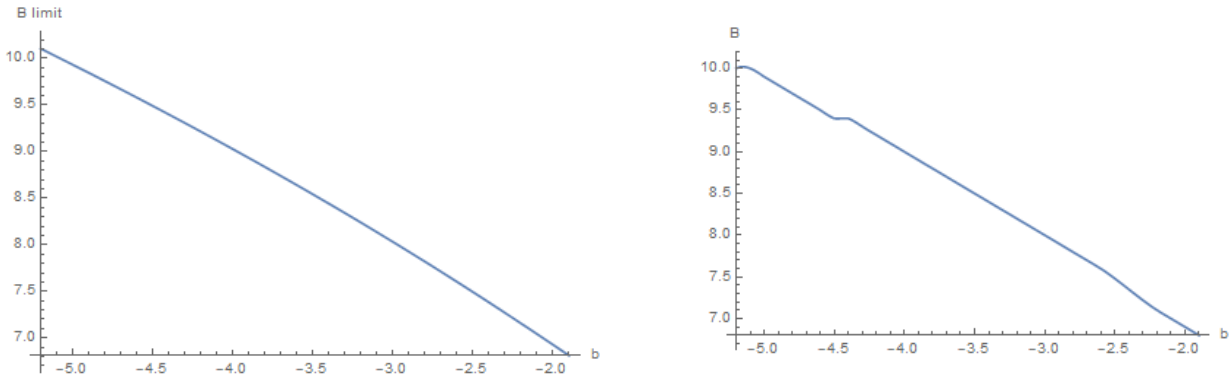

FIGURE 4.10: On the left we have the limit found for the maximum value of B, while on the right we have the $T = 0$ line which was extracted numerically.

For $\boldsymbol{b > 0}$ the temperature behaves rather differently as shown in figure 4.11. In this case the temperature is tending towards zero in a small range of b when compared with the range of B, as both parameter ranges are increased the $T \sim 0$ line continues to extend increasing in both B and b.

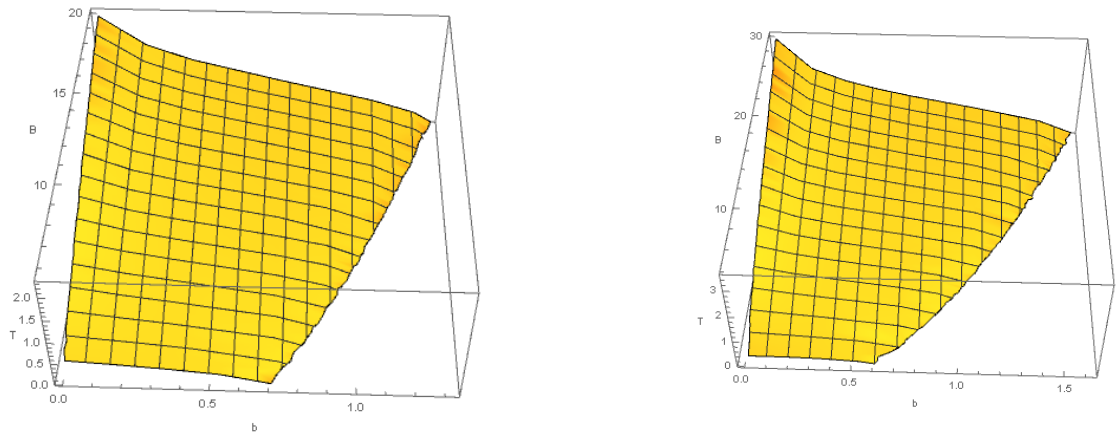

FIGURE 4.11: Temperature profile for $b > 0$. In this case the line where $T \to 0$ grows as B increases and b decreases.

This behaviour is quite interesting as the trajectory of the region changes early on in the parameter values, but then retains a steady trajectory afterwards.

In this case the limit found on B does not correspond to the $T \sim 0$ line, but we could extract a numeric expression.. Again the $T \sim 0$ line is approximately the boundary of the the region, which we plot below in figure 4.12. This was found by computing the temperature over a range of B, b values, and locating the combinations that resulted in a temperature of approximately zero ($T < 10^{-3}$). This approximated the region quite nicely, as one would hope.

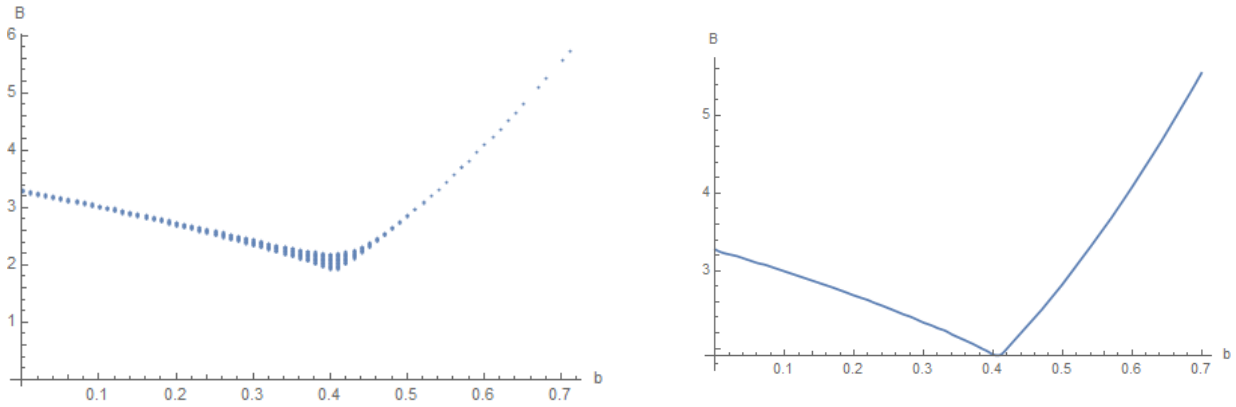

FIGURE 4.12: The approximately $T = 0$ line for $b > 0$.

4.5.3 Quasinormal modes

The findings of the previous section mean that the temperature is now a function of b, χ and B, and all that is left to do is to use equation 4.33 to eliminate b. When calculating the modes, we can use equations 4.30 and 4.31 to get the fluctuation equation in terms of just B, b and χ, and χ can be set to one for our purposes. Therefore, since this is all we need to compute the modes, the modes are a function of B and b. Similarly, the gap equation, as given in 4.33 is a function of B and b, so from this equation we should be able to find $b(B)$ and substitute this into our equations so that the only parameter is the magnetic field. The Mathematica package used to calculate the modes does not return an explicit formula for $\omega_I(b, B)$, we can numerically find the root of equation 4.33 and numerically solve for b.

We want to find $\omega_I(b, B)$, so we need to compute the modes over a range of b and B values, this function is a surface, and equation 4.33 is just the intersection of this surface with the one created by the

gap equation. We can then find a numerical representation of the equation of this intersection which will determine $b(B)$. We will start with the $b < 0$ case and then move on to the $b > 0$ case.

$b < 0$ case

To begin, we first need to compute all the quasinormal modes over a suitable range of parameter values. To do this, we modify the code to loop over all values of b and B, subject to the condition 4.29. The smallest horizon solution per loop that satisfies this condition is then chosen as the horizon value, and the code returns the lowest quasinormal mode for that horizon. From here we make a table of all the modes and their corresponding b and B values, and use this table to plot the resulting surface. Due to the fact that there is a limit on the value B can take, we had to be careful when choosing parameter ranges, as computing the modes even near the 'bad' values could result in numerical errors affecting the results. To overcome this, we first found all the parameter combinations that resulted in a positive real temperature, which also satisfied the horizon conditions. This ensured that only good combinations were evaluated, and also massively reduced the computation time.

The code was ran over the ranges $-15 < b < -1$, and $1 < B < 15$, and figure 4.13 shows the result.

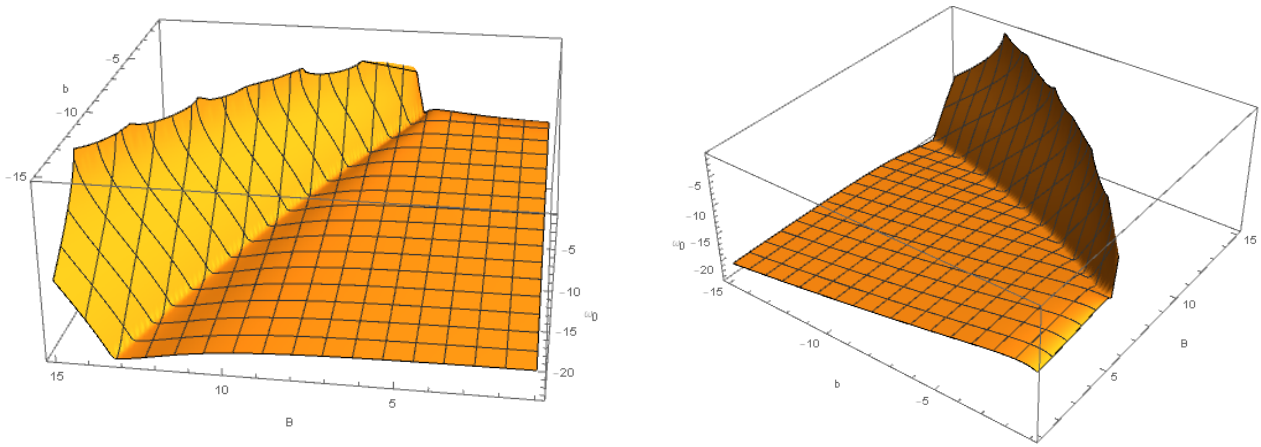

FIGURE 4.13: $\omega_I(b, B)$ for $b < 0$

Interesting behaviour of the fundamental mode can be observed; as B is increased, it is relatively stable until at some point it begins to steeply increase towards zero. Recalling that the fundamental mode in inversely proportional to the characteristic timescale for the perturbations, we see that there is a sudden change in the timescale occurring. We know that in a quantum phase transition, the two phases are distinguished by different equilibration times, and so this plot seems to be indication this change and hence at the phase transition taking place.

Recalling the behaviour of the B limit 4.7, 4.10 and the $T \sim 0$ line 4.11, we can see that the stability change seems to coincide exactly with these curves. The modes were computed with the temperature ($\omega = 2\pi\lambda T$), so it would be expected that they should approach zero as the temperature does.

Looking at the $b = -6$ slice in figure 4.14, we can identify two important regions; at around $B = 8.7$ the modes become very negative, while at approximately $B = 9.5$ the modes become very close to zero. Since the modes are inversely proportional to the equilibration time, we see that these regions have very different equilibration times. Namely the first has a very short equilibration time, and is seemingly stable, whereas the second has a very long equilibration time which suggests that at this value of B the system is unstable. Considering our discussion in the previous paragraph, this seems to imply that along at least this section of the $T = 0$ line, the system is quite unstable, but as T is increased the stability increases. We see though that for smaller values of b the stability increases faster than for larger values, which could be a result of the smaller vacuum expectation value introducing less instability than

a larger one would.

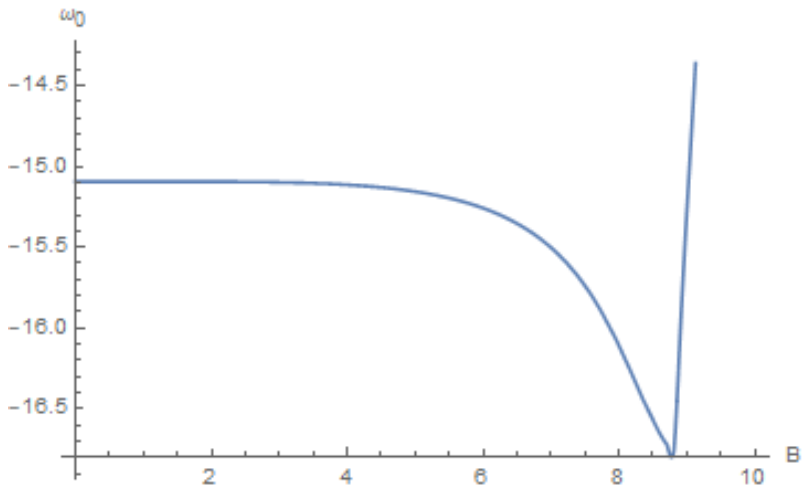

FIGURE 4.14: $b = -6$ slice of the fundamental mode behaviour. Here we can see the two regions of interest, one having a very long equilibration time and the other a very short equilbration time.

To estimate where the transition is taking place we will try to figure out where the boundary of the regions is. We can do this with equation 4.33, using the appropriate expression for b_{TG}. We run into difficulties here however as we do not know the exact proportionality of the relationship. To see the approximate region of the intersection, provided the proportionality factor is not too large, we plot equation 4.33 as it is, shown in figure 4.15. There is an intersection, which is good news for the phase transition, however in this situation we do not know for sure where exactly the QCP is, as the thermodynamics analysis previously undertaken was only done for $b > 0$. We expect however that it should be should intersect this line somewhere, so in this case it would probably be for a larger value of B than for the $b < 0$ case. This of course all depends on where exactly the intersection is taking palce, but it woluld be expected that it would meet the $T = 0$ line somewhere, which we think is defined by the edge of the 'fin' part of the modes. This effect of the negativity/positivity of the VeV on the stability of the system would be an interesting result, but for the moment we cannot say for certainty what happens. So until we work out these details of the duality transformation and the thermodynamics, we cannot do or say much more.

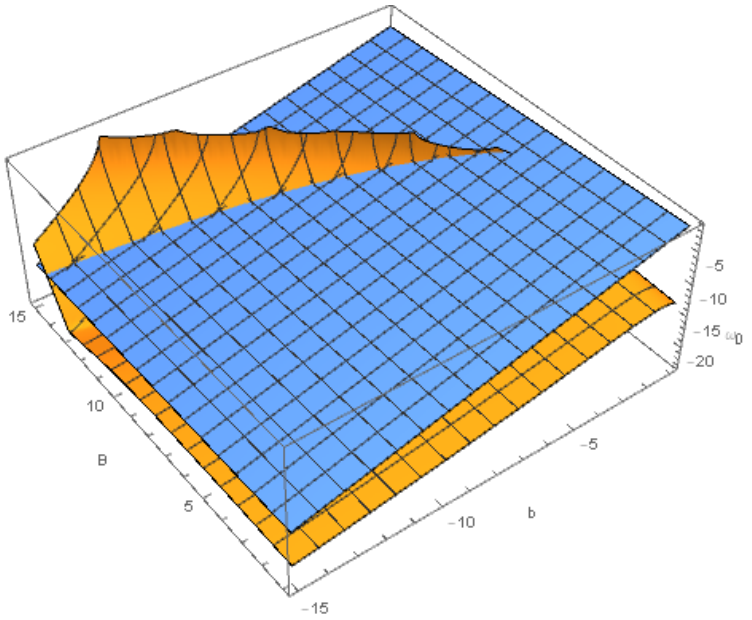

FIGURE 4.15: Boundary of the quantum critical region in the b, B plane for $\chi = 1$ slice.

$b > 0$ case

Now we carry out the same analysis for $b > 0$, the only difference in this case is that the horizon must obey the second lower-bound as given in 4.29, and we have $b_{\text{TG}} = 2^{-\frac{7}{2}}\sqrt{|B|}$. For the fundamental mode we get the following behaviour shown in figure 4.17. For this case the range we executed the code over was $.01 < b < 15$ and $.01 < B < 15$.

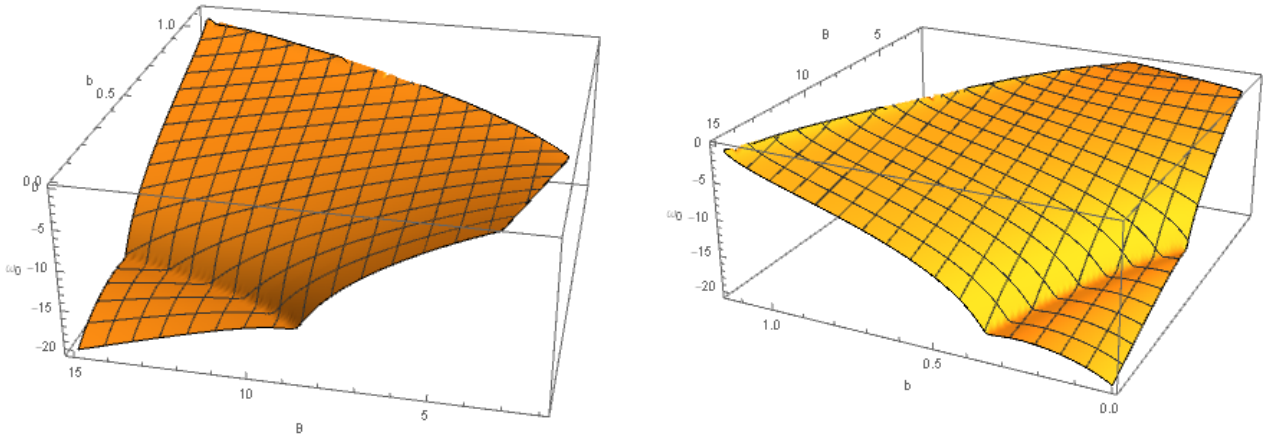

FIGURE 4.16: $\omega_{\text{I}}(b, B)$ for $b > 0$

This case shares similarities with the previous, as we have a similar change in the mode behaviour, where they are quite close to zero for many of the values, however as b decreases we see that the modes become more and more negative, and as we increase the range of the parameters we find that for larger values of B the modes do indeed become increasingly negative. This all in turn means that again we have clear changes in the equilibration time taking place, the system being quite stable in on region to being unstable in another. So this suggests again that we have a phase transition taking place.

Taking a slice at $b = .2$, we can see how the modes get quite close to zero for small B values, showing the instability of this region, while for large values we see that the system is quite stable. The image on the left shows how the equilibration time is change along this slice.

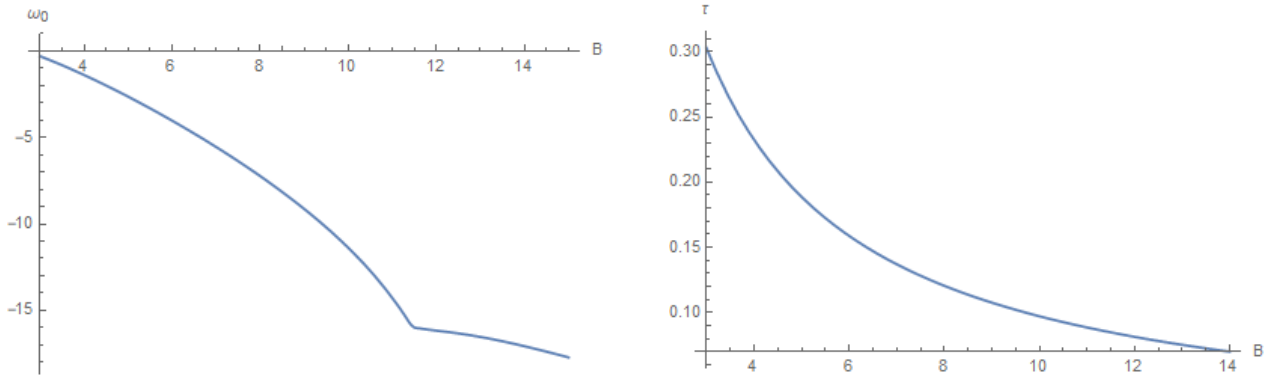

FIGURE 4.17: On the left is a slice of the fundamental mode behaviour for $b = .2$, and on the right is the equilibration time over this region. We see near $T = 0$, for small B values, the system has a very long equilibration time and so seems to be unstable. As we increase B the stability increases, this change suggests the presence of the QCP.

As with the previous case, we can see that the $T \sim 0$ line is actually defined by the boundary of the modes as they approach zero. Comparing the behaviour with that of the temperature in figure 4.11, this relationship can clearly be observed, the shape of the mode boundary replicating that as shown in figure 4.12. Figure shows both the temperature and mode plots together, where the relationship can clearly be seen. Again, this relationship is the be expected as the modes are proportional to the temperature.

To get a better idea of what is going on, we can try to determine where the quantum critical region is, using equation 4.33. Figure 4.18 shows this this intersection, and hence where the quantum critical region should approximately lie. We see that the intersection is only in a very small range of b values, as mentioned before, equation 4.33 is not necessarily an exact equation, there is possibly a constant of proportionality there that could shift the region one way or the other, so this location may not be entirely accurate. A good sign though is that the QCR boundary does seem to end on the $T = 0$ line, and approximately at B_c.

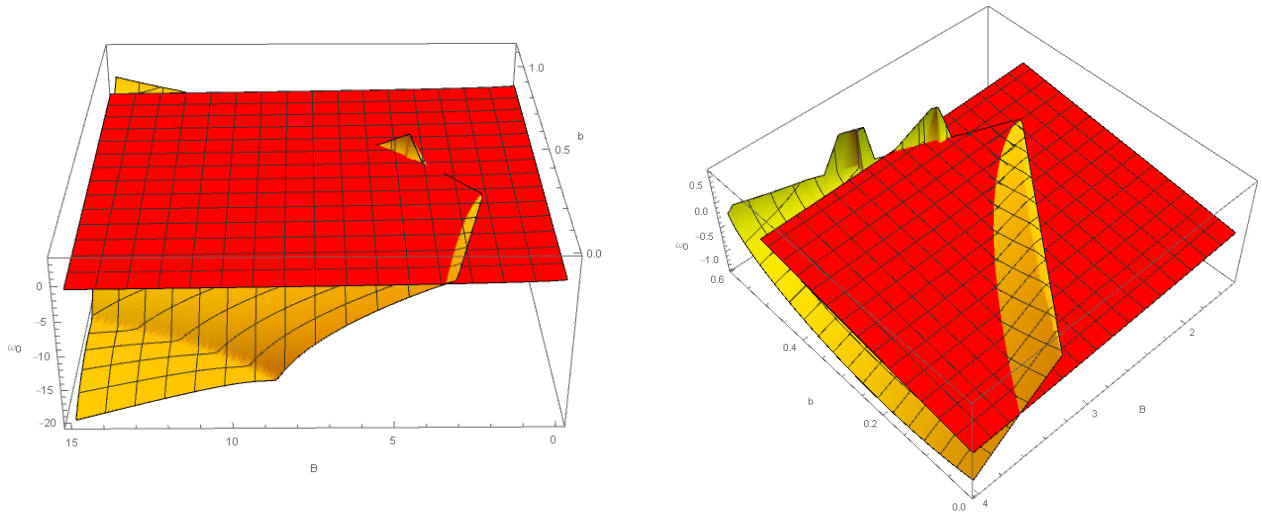

FIGURE 4.18: $\omega_I(b, B)$ for $b > 0$. On the right, a close up of the intersection is shown, indicating the location of the quantum critical region.

Now, all that is left to do is to see if we can extract the dependence of b on B from this intersection and use this equation in our temperature equation so we can see how the temperature changes with the magnetic field.

Multiple attempts were made to numerically extract the b, B curve, most of which were unsuccessful. The initial goal was to interpolate the table defining the intersection, numerically find the roots of this and solve for $b(B)$. Most issues with doing it this way were arising from the fact that the curve is over such a short region for very small parameter values, such that interpolating the function was not possible. Increasing the step size allowed us to attain an interpolating function of the intersection, however the resulting b, B curve was not accurate when compared to what we could see, so this method was not acceptable. Instead, we chose to take the intersection table, and extract all the instances where the temperature was approximately zero ($T < 10^{-3}$) and their corresponding B and b values. Plotting these values, as shown in figure 4.19 shows a relationship more like what we can see from figure 4.18.

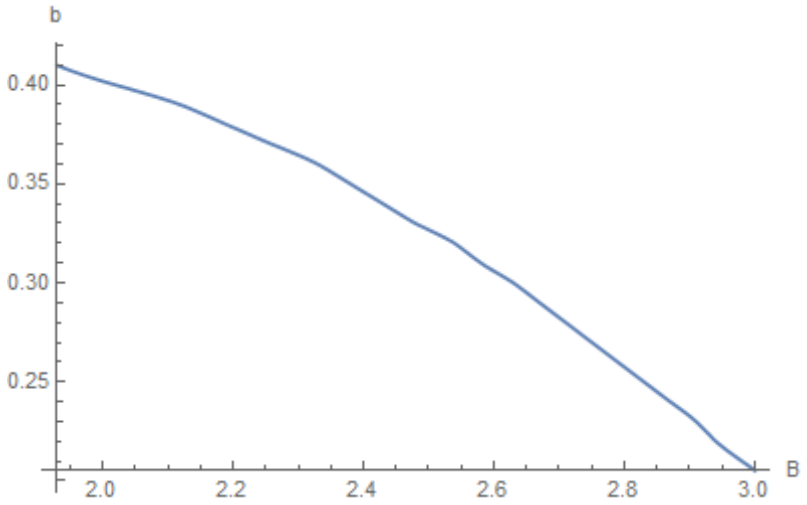

FIGURE 4.19: Relationship between b and B along the quantum critical region.

The downside of this intersection, is that it does not intersect a large section of the $b - B - \omega_I$ phase space. It ranges over a very small subset of B values and so we can only make use of the $b(B)$ equation over this range. As stated earlier, it could be that this intersection is actually not exactly in this position, due to the proportionality factor in the τ_{eq} equation. So this intersection could possibly be valid over a larger range of B values. What is strange however, is that the $T \sim 0$ line seems not the extend past the critical point, and neither therefore do the modes, and so our quantum critical region boundary also cannot attain any values beyond this boundary. This seems strange, and requires somemore thought, and is something which we will try to figure out in the near future.

Nonetheless, we will make use of this equation and see what it gives us. Plugging the numeric $b(B)$ expression into the temperature equation 4.48 and plotting, we find the phase diagram shown in figure 4.20.

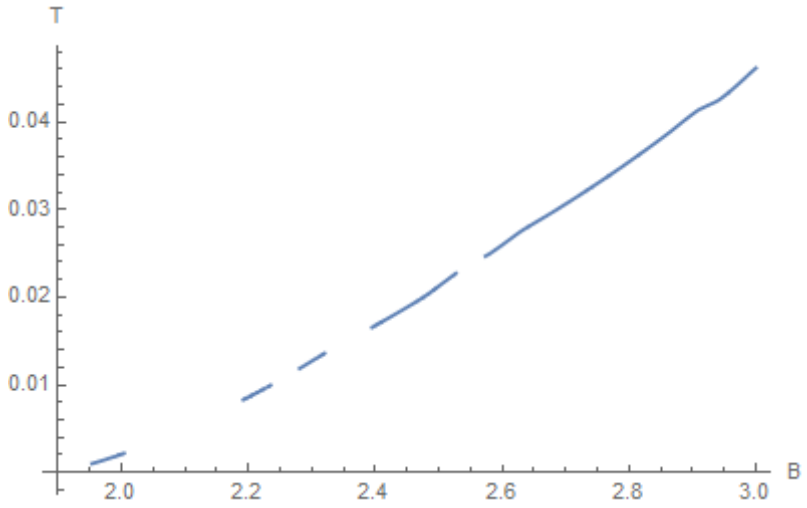

FIGURE 4.20: Section of the $T - B$ phase diagram for $b > 0$

This phase diagram seems to be what we expect; we know that the quantum critical point is located at $B_c \approx 1.9$, and that is what we are seeing here, the temperature looks like it is going to be zero at around that point. Now the obvious thing we are missing is the other side of the critical point, and this is not visible to us due to the way we determined the $b(B)$ equation, namely we used the intersection, which only ranges over a very small section of B, and so the allowed range for this equation is quite restricted. Another equation might give us the full $b(B)$ range, but as mentioned earlier, it seems that the boundary of the region is not extending past this critical point, but one would expect that it should extend past this point. Consequently, more analysis needs to happen to fully understand the reasons why this is happening.

Chapter 5

Discussion and outlook

5.1 Discussion of results

Here we will recap on what did and what we found.

Our goal was to use the quasinormal modes to investigate the quantum critical point and the surrounding region. Computing the modes from the fluctuation equation allowed us to find the quasinormal modes as a function of B, b and χ. We were interested in the behaviour of the fundamental mode, as this was the one from which we could determine the equilibration time for the dual field theory. To understand the changes taking place in the field theory, we determined the behaviour of this fundamental mode over a range of the parameter values, and for two cases: $b < 0$ and $b > 0$. Figures 4.17 and 4.13 display this behaviour. In both cases it is clear that a distinct change is occurring in the behaviour, and hence the equilibration time of the field theory. From our discussion in chapter one about quantum phase transitions, we know that this is suggestive of the presence of the quantum phase transition taking place. The behaviour of fundamental mode showed clear regions where it was getting close to zero, and so corresponded to increasing instability in the field theory, and other regions where it became quite negative, revealing where the system was stable. Interestingly both cases had quite different shapes.

Performing an analysis of the temperature behaviour over the same range, revealed interesting trends; first we were able to see where approximately the temperature was vanishing, and we saw that this corresponded exactly to where the modes were tending to zero and hence where the system was becoming increasingly unstable. This is expected however as the temperature is used to compute the fundamental mode. The second thing that was interesting to note was that in the $b < 0$ case, we were able to analytically determine an upper limit on B, which corresponded to this region where the temperature was vanishing, and so we have an analytic expression for the boundary in the B, b, ω_I plane. In the $b > 0$ case, we were not able to find an analytic expression for the $T = 0$ line, but we could numerically extract it and confirm that it corresponded with the boundary of the fundamental mode.

The final task we tackled was to try to use all this information to determine the boundary of the quantum critical region. Using the boundary equation we found in chapter three (equation 4.33), and our analytic expression for the temperature in both b cases, this should be possible. In the $b < 0$ senario, we had the limitation that we didn't have the exact equation relating b_{TG} and B, namely we were missing a proportionality term and so the exact intersection equation is not known. However, just to get a rough idea of what was happening, we took the proportionality to be one to see where approximately the boundary might be. Figure 4.15 showed this. We see that an intersection takes place in this case, and as long as the proportionality difference is not very large the actual intersection should occur in a reasonable place. This case definitely needs further analysis however, as in the current trajectory of the boundary, it does no seem to reach the critical B value, and it is probably a result of the proportionality problem.

The $b > 0$ case was a bit more promising and utilisable, the intersection being as shown in figure 4.18. The only problem here was that the intersection occurred over a very small parameter range in b, affecting the numerical methods we were using to extract information, and also restricting the equation

we found relating B and b. Here we could see that the boundary terminated where we approximately knew was the $T = 0$ line. This intersection also ended at what seemed like the QCP. Using our expression for the temperature, we were then able to see the temperature behaviour as a function of the magnetic field, but only over this small parameter range. This is shown in figure 4.20, and it displays somewhat expected behaviour; we can see what looks like half of what is typically expected to be the shape of the QCR, and it terminates at what we know should be the QCP, given by equation 4.16. We are of course missing the other side of the boundary. As a result of using the intersection to determine the B dependence of b, we were limited in the range of B values we could use this relationship over. It seems to be that the boundary of the quantum critical region does not extend past the QCP, which seems strange, but with our identification of what seems to be the $T = 0$ line, it doesn't seem possible that that could occur anyhow. Looking at our $T = 0$ line, the QCP does intersect it, as one might expect, but the rest of the line does not extend past the QCP, instead it seems to go back in the same direction.

Another aspect that could be affecting this however is the proportionality that might be involved in the boundary equation we found (equation 4.33), so this should also be considered. It is clear then, that more analysis and thinking needs to be done about this situation, and that will be our next step.

5.2 Outlook

There is clearly much more analysis that needs to be done to better understand the dynamics that are going on. We will continue to work on this problem after the actual thesis is officially over, where we hope to think more about what we found, improve it, and take the analysis further.

For a start, the one of the first things that should be done is to determine the exact identification between the charge and magentic field, so we can properly analyse the intersection for the $b < 0$ case. The next thing we should do is determine a better equation for $b(B)$ that includes both sides of the critical point, so we can see the the full behaviour around the QCP.

Something else we attempted to do but did not have enough time to finish before the thesis deadline, was the computation of the metric, gauge, and scalar quasinormal mode spectra. Therefore this is someting which we will find next, and should illuminate the siutation further. Also, from this we will be able to compute quantities such as the conductivites for the system. Analysis of the finite temperature thermodynamics of the system should also be carried out, to search for any thermal phase transitions that might be taking place. These are the future goals, which we hope to tackle in the coming months, building upon and better understanding what we already have.

[heading=bibintoc]

Bibliography

[1] S. A. Hartnoll. Lectures on holographic methods for condensed matter physics. *arXiv:0903.3246 [hep-th]*, 2010.

[2] Subir Sachdev. *Quantum Phase Transitions. (Second Edition)*. Cambridge University Press, 2011.

[3] J. M. Maldacena. The large N limit of superconformal eld theories and supergravity,. *[arXiv:hep-th/9711200*, 2 1998.

[4] G. 't Hooft. A planar diagram theory for strong interactions,. *Nucl. Phys. B 72 461*, 1972.

[5] S.W. Hawking. Particle creation by black holes,. *Commun. Math. Phys. 43, 199*, 1975.

[6] J. D. Bekenstein. Black holes and entropy,. *Phys. Rev. D 7, 2333*, 1973.

[7] I. R. Klebanov S. S. Gubser and A. M. Polyakov. Gauge theory correlators from noncritical string theory,. *Phys. Lett. B428 105*, 1998.

[8] E. Witten. Anti-de sitter space and holography,. *Adv. Theor. Math. Phys. 2 2535*, 1998.

[9] L. Susskind and J. Lindesay. *An introduction to black holes, information and the string theory revolution: The holographic universe,*. World Scientic, 2005.

[10] S. Hod. Universal bound on dynamical relaxation times and black-hole quasinormal ringing,. *Phys. Rev. Lett. 81, 4293*, 1998.

[11] A. O. Starinets E. Berti, V. Cardoso. Quasinormal modes of black holes and black branes,. *arXiv:0905.2975 [gr-qc]*, 2009.

[12] A.O.Starinets D.T.Son. Minkowski-space correlators in ads/cft correspondence: recipe and applications,. *arXiv:hep-th/0205051,*, 2002.

[13] A. Jansen. *Black holes and oscillations,*. ProefschriftMaken, 2018.

[14] O. Papadoulaki C. Toldo A. Gnecchi, U. Gursoy. A magnetically induced quantum critical point in holography,. *JHEP*, 2016.

[15] Daniel Louis Jafferis Juan Maldacena Ofer Aharony, Oren Bergman. N=6 superconformal chern-simons-matter theories, m2-branes and their gravity duals,. *arXiv:0806.1218 [hep-th],*, 2008.

[16] E. Witten. Multi-trace operators, boundary conditions, and ads/cft correspondence,. *JHEP*, 2002.